1. **Broadband radiance determination:** It is interesting to consider the possibly of using IASI data to this end and the method employed differs somewhat in detail from exiting narrow-band to broadband techniques. However, the authors make little mention of existing progress in this area and the method falls short of delivering the expected level of accuracy of multichannel techniques covering this spectral region (e.g. Ellingson et al. 1989) and seems only to achieve similar results to exiting methods based on much more limited spectral observations from two narrow-band channels in the window and water vapour bands of AVHRR or METEOSAT (see for example Gube 1982; Schmetz and Liu 1988; Cheruy et al.1991; Minnis et al. 1991; Gruber et al., 1994;). It is difficult then to see what the proposed method offers over these established techniques, which in many cases included the additional determination of the flux. The authors need to do more to highlight the advance of their approach and properly put it in the context of this body of work.

Page 5, line 28 – page 7, line 14 reviews the existing body of work on narrowband to broadband techniques. This originally concentrated on polar orbiting satellite instruments, however we have extended this to include lines 15-18 on page 6, and added a new paragraph on the geostationary instrument studies that the reviewer mentions (page 6, line 26 to page 7, line 17). We have added a paragraph and two figures to the methodology section that quantify the accuracy of the regression model (page 11, line 28 to page 12, line 8) and produces a total relative error of 0.15%, which we believe exceeds the accuracy of existing similar methods. However producing a surrogate broadband instrument is not the focus of the study, which is detailed further in answer to the reviewers 3rd point. The proposed method is unique among others in that it resolves the far infrared (and near infrared) at high resolution, utilising the full breadth of the spectrally continuous IASI range, and the paper is refocused with this aim in mind, see particularly the abstract.

2. **Retrieval of simulated spectra:** As far as deriving spectral detail is concerned, it is obvious the method cannot add any additional information to the IASI observations beyond model assumptions. However, the technique described could plausibly provide a valuable shortcut to reconstructing simulated spectra and offer an alternative to for example simulations based on retrieved information from IASI. The authors need to clarify this aim and evaluate the ability of the method in achieving it, considering its strengths and weaknesses over the alternatives such as performing an explicit retrieval to provide

input to a simulation. As it stands the authors fail to demonstrate, even **theoretically**, how well the proposed method performs in this regard.

The validation of the technique's ability to provide a reasonable estimate of broadband radiance does little to validate its spectral fidelity: there is a difference between spectrally important features and their radiative impact and compensating errors in different spectral regions, which have been seen in previous model comparisons (see Huang et al., 2006), cannot be diagnosed by such broadband validation.

Furthermore a discussion of correlations does not enable the distribution of residuals to be inferred for each wavelength, nor inform on the ability of the model to capture the variability of the true atmosphere. It is clear that the empirical relations derived from the simulated spectra will provide an imperfect reconstruction, whilst the variability in the correlation coefficient shown in figure 4 leads to the expectation that the errors will have spectral structure (note: although this figure is described in the text as containing the regression coefficients it actually appears to contain the correlation coefficients). In addition, noise on the IASI observations and any deficiencies in the simulations ability to model the IASI region will also impact how well the simulated spectra can be reconstructed. These factors are not considered, either in selecting the optimum channel predictors or in evaluating the fidelity of the reconstruction. These effects should be quantified; the theoretical fidelity and robustness of the reconstruction demonstrated and its performance evaluated under different conditions and for different scenes. Its sensitivity to the expected noise in the IASI observations also needs to be determined. It would make sense that these studies also consider the optimum spectral resolution of the reconstructed spectra, taking into account the ability of the method.

With the lack of any space borne far infrared measurements in existence with which to calculate empirical relationships, we are limited to theoretical methods in constructing the regression model. We have added text that states these limitations within the bounds of the line-by-line code, LBLRTM, which we believe is the most accurate tool available for our purposes (page 8, lines 12-18). This is re-iterated in the conclusion, page 20, lines 5-10. The quantification of theoretical model errors described in answer to the reviewers 1st point demonstrates how well it performs. The unfiltered CERES total longwave radiance provides constraints on the total radiant energy, which effectively is a comparison of the FIR and NIR regions,

assuming the radiant energy from the overlapping observable range are in agreement between CERES and IASI. Naturally this assumption involves the accuracy of both instruments, calibration differences and unfiltering processes. The biases found in Section 3 are partly attributed to these factors, and are all well within the expected errors (page 15, lines 22-24).

While not evaluating the individual spectral lines individually the broadband comparison is the most independent observational test, because the algorithm is not constructed with broadband targets but spectral ones, i.e. no broadband observations are involved in the training of the INLR product. The fact that the two products are so close in values provides us with confidence in the applicability of this algorithm. It is unlikely that the broadband fidelity is due to compensating biases along the spectrum given this lack of 'tuning'. Theoretical errors arising from the log-log regression model are small (see fig 5 in revised paper), Thus, biases arising from deficiencies in LBLRTM, and cloud properties, in the FIR would need to sum to close to zero given the agreement between our IASI product and CERES data. This suggests that over the FIR as a whole our reconstruction is accurate. That does not preclude errors within the FIR which would need direct observations of the FIR to evaluate, a development we would be pleased to see.

The Huang et al. 2006 paper that the reviewer mentions, *Quantification of the source of errors in the AM2 simulated tropical clear-sky outgoing longwave radiation,* is a global climate model evaluation study where compensating errors arise due to fundamental problems with the simulation of climate model atmospheric fields and their wideband radiation schemes, which is a different problem to the spectral radiance reconstruction model addressed here, using radiosonde observations and a line-by-line model which are far more accurate.

The spectral structure of the models rms errors are shown in Figure 5, right hand panel, and the relative errors are shown in Figure 6. In terms of relative error there is little dependency on wavenumber. The model is constructed using 3200 soundings which have been shown by past studies to fully capture the wide variability of atmospheric scenes and conditions (text added on page 10, lines 25 to 28. The stratification of scenes, simulations with built in instrument errors, and expanded regression model form are all refinements that could further improve the performance of the technique, however the purpose of this study is to demonstrate the

feasibility of this technique, not argue it has reached the optimal stage, which could be done in future studies. This is presented in the conclusion, page 20, lines 5-13.

3. **Clarity of the aim and model details:** In parts of the paper the authors seem to lose sight of the fact that the method they propose is a shortcut to derive a model based simulation from the information contained in the IASI observations. The authors discuss in the introduction (page 18423 line 12 to line 6 on page 18424) the importance and uniqueness of the far infrared, the additional information in can potentially provide on upper tropospheric water vapour compared to the mid-infrared, the poor understanding of the water vapour continuum at these wavelengths and observational and modelling discrepancies in this spectral region and conclude that greater understanding and long term observations in this spectral region are needed. These are excellent points and are well illustrated by the references given. I would add to this that the models ability to correctly reproduce the far infrared spectral signature of cirrus which as the authors note is of particularly significance for this spectral region, will also be limited, given both the difficulties in simulating these properties and the potential for unique information about these clouds to be contained in the far infrared (Di Giuseppe and Rizzi,1999; Yang et al., 2003, Baum et al., 2014). The method presented in the paper to reconstruct simulations of the spectral regions not observed by IASI will of course include all the deficiencies and uncertainties of the original model of the type discussed above and will not add any additional information to that contained in the IASI spectral range except those of the model assumptions. Thus, although it is not explicitly stated, this discussion is of the limitations of their technique and it would seem to be in need of a counter augment from the authors on why the technique is nevertheless of use.

We agree with the reviewer that it is unlikely the model will be able to capture the spectral signature of cirrus clouds, given the limitations of the LBLRTM model in its treatment of clouds. Validation of this aspect of the LBLRTM model is something that is lacking in the literature, in contrast to extensive validations of clear-sky parameters such as the water vapour continuum, and this is certainly something that this product could benefit from in the future. We have added text on page 19, line 26 to page 20, line 4 to caution applications that might be sensitive in this regard. The text states how this study strengthens the case for a spaceborne far infrared instrument, in order to develop the model to allow more detailed analyses.

4. Consideration that the resulting spectra retrieved are limited by the model used and all the results discussed in section 4 are specific to this model and its assumptions (plus subject to additional errors introduced by the method employed to reconstruct the spectra) is also lacking in the presentation of section 2.2 and section 4. Hardly any information about the modelling input and assumptions are provided, all that is stated is that LBLRTM is used along with radiosonde data from 1600 soundings with a second set of cloudy simulations performed by random insertion of a cloud layer. Where are the radiosondes from and do they cover the full variability in the atmosphere? What cloud properties are used, are the cloudy atmospheric profiles different from the clearsky? How are the cloud properties determined? How are ice particles modelled? What particle size, shape and water content are used in the simulations? Is scattering included? What surface properties are used? How well do the simulations match IASI observed spectra? Maybe such questions are of less importance for a proof of concept only, but the results in section 4 are entirely dependent on these issues, they are a demonstration of what this model says is going on in the far infrared given information on the atmosphere from IASI. It is not appropriate to include and discuss these results without this context.

Full details of the input radiosonde data have been added to the methodology on page 10, line 25 to page 11, line 14. High level clouds are assumed to have the spectral properties of cirrus given by Haurwitz and Kuhn (1974). As said in answer to the reviewers second point the stratification of scenes, simulations with built in instrument errors, and expanded regression model form are all refinements that would further improve the performance of technique, however the purpose of this study is to demonstrate the feasibility of this technique, not argue it has reached the optimal stage, which could be done in future studies. This is presented in the conclusion, page 20, lines 5-13.

Page 3, Lines 27-28: I would recommend changing "in a warmer world there will be an increase in water vapour due to its positive feedback" to something like "Because the relative humidity is expected to remain constant, the water vapor mixing ratio will increase in a warmer world."

We agree with the suggested change, page 3, lines 26-27

Page 8, Line 28: Citing Loeb et al. (2003) for the ADMs is fine, but I would recommend also citing Loeb et al. (2005), since it describes the ADMs used for the CERES instruments on Terra and Aqua.

We have added this reference and Clerbaux et al. (2003), page 8, line 28

Page 11, Lines 6-7: CERES footprints are not generally referred to as pixels in order to differentiate CERES footprints from MODIS pixels. In any case, the footprints are not circular (even at nadir), closer to an extended hexagon (see Fig. 3 of Smith 1994).

We have amended the text and removed the words pixel and circular, page 12, lines 15-16

Page 12, Lines 1-2: Although flux and radiance are proportional for a given scene, anisotropy varies significantly between different scene types. This is especially true for nadir-viewing scenes such as those in this study.

Agreed, the quantity we are comparing is the broadband LW radiance from CERES, for which uncertainty estimates are not provided, only for the flux quantity which includes errors from the radiance-to-flux conversion. Hence are uncertainty estimate has an upper bound of 1.5% (the flux uncertainty) and will likely be below this. We have rewritten the text to reflect this, page 13, lines 3-12

Page 13, Lines 20-22: It is good to point out that the radiosonde data used for the correlation analysis is based on tropical and mid-latitude soundings, but the sentence (as written) seems to imply that if the algorithm works for polar latitudes (where it isn't "supposed" to work), it will surely work for middle and low latitudes as well. Please rewrite.

We have removed this sentence entirely as it is confusing. We have given more information on the locations of the radiosondes in the methodology (page 10, line 26 to page 11, line 15) which are between 30S to 60N. The algorithm is robust at different latitudes.

Various places in Section 3: Differences between IASI and CERES are expressed as CERES minus IASI. Since CERES (with its measurement of broadband LW radiance) is treated as the truth in this comparison, I would suggest changing to IASI minus CERES.

We agree that CERES is taken to be more truthful in this context, however, for the sake of retaining a positive quantity for the duration of the study, we prefer to express it as stated.

Section 4.2: The increased proportion of Far-IR energy for cloudy scenes is interesting. Much of this is due to the shift to a lower emitting temperatures (and hence, lower peak wavenumbers according to Planck's Law) for cloudy scenes, as noted earlier in the manuscript. Is there a way to quantify the departures from the expected shift with temperature?

The reason that the proportion of FIR energy increases relative to that in the clear sky case is because that the cloud effect (reduction of thermal emission to space) is stronger in the other part of the spectrum, especially in the atmospheric window. This distribution of total LW energy to a certain band, e.g., FIR, depends on the given atmospheric composition and the knowledge of molecular spectroscopic properties and the cloud optical properties, all as functions of the frequency. Quantification of this is possible, but assumptions of cloud optical properties will play a major role. It can be expected that it will be different for the near opaque water clouds and for the more transparent cirrus clouds. The algorithm provided here will enable us to use IASI observations for such evaluation and quantification.

Page 20, Lines 6-10: As noted earlier, the isotropic assumption is not particularly good, especially at nadir. However, it could be noted that the error estimate resulting from this assumption is likely high, since the anisotropic factor at nadir is greater than 1.0 for almost all scene types (the coldest nighttime scenes in Antarctica being an exception). Please be more specific with the statement that these flux differences are "comparable in magnitude to those presented in previous studies.."

We agree that the equivalence between flux and radiance is not straightforward, and have removed this sentence from the text. The comparison with radiance is the most direct comparison. We have added a paragraph in the introduction that clarifies the distinction, page 8, line 20 to page 9, line 9.

Technical Comments Page 4, Lines 12-13: Not sure what is meant by "clear to cloudy instantaneous conditions."

The instantaneous refers to a single measurement, rather than globally or time averaged. It has been removed from the text

Page 6, Line 3: With Pluto’s demotion to dwarf planet status, you can remove the "and Pluto" from the text.

Page 7, Line 16: Should be "principal component analysis".

Figure 9: The "Locations" in the figure panels give two latitudes. I assume that the number followed by S should be followed by an E instead?

Page 17 and Figure 10: "Peak wavelength" is given in terms of wavenumber.

Page 19, Line 7: Change "Interesting" to "Interestingly".

These amendments have all been made and we thank the reviewer for alerting us to these errors.

1. **Incorrect assumption of isotropic radiation** Based on radiation transfer equation, it can be easily shown that in general case the upward radiance field at the TOA is not isotropic. Thus spectral flux cannot be computed accurately by simply multiplying a factor of pi. The author supported the usage of this incorrect assumption by stating the globally average difference between CERES-IASI OLR is small. But this heavily averaged difference over the entire LW spectrum cannot justify the usage of this assumption at all, for so many compensating error sources can contribute to this broadband flux difference (I will discuss in detail about this in Comments #2 and #3). In atmospheric radiation, there is a widely used and well established approximation, the diffusivity approximation, which can be found in nearly all the atmospheric radiation textbook. It states that the flux can be approximated by the radiance at 53 degree (diffusivity factor 1.66) multiplying pi. This diffusive approximation has been first introduced by Elsasser in 1941 by examining the radiation chart and has been widely used ever since, in both observation and modeling. Li (2000) gave theoretical explanation of this approximation. Virtually all the GCM radiation schemes employ this approximation to compute the LW flux since they cannot afford to compute radiance at multiple zenith angles and then integrate them to obtain flux. If what the authors used in this study were true, it would be equivalently saying that this well established diffusive approximation were wrong and every scheme could simply compute radiance at nadir view. Such direct contradiction to the well established and well verified approximation to compute LW flux is not even mentioned, let alone justified or proved. Furthermore, in one reference cited by the authors, Huang et al. (2008) clearly shows how each spectral channel can deviate from the isotropic radiation assumption for the clear-sky situation. Figure 2 in Huang et al. (2008) shows that, in some spectral channels, the anisotropic factor is as large as 1.2, which means that a 20% error would be introduced if the spectral flux of such channel were estimated as in this study. Note the same Figure 2 in Huang et al. (2008) also corroborates that the anisotropic factor for the diffusivity angle suggested by Elsasser is indeed much closer to one than that of nadir view angle for all the LW spectral channels. In another reference cited by the authors, Huang et al. (2006), such nadir view radiance from old dataset IRIS was used to multiply with pi in the second part of the study. But Huang et al. (2006) carefully defined it as “nadir flux” and used this term in all figure captions and relevant discussions to distinguish from OLR or flux as commonly defined. The“nadir flux” was never used to compare with actual OLR observation or OLR simulation in the entire text of Huang et al. (2006). In a nutshell, it is

fundamentally wrong to compute OLR in the way done in this study. It contradicts well-established and well verified diffusivity approximation and the equation of LW radiative transfer. The author failed to show any proof why they can do so. The “flux” derived in this way has a dimension of flux, but physically is not the same quantity as the OLR obtained by CERES or simulated by any GCMs. Thus, all the consequent comparisons with CERES OLR and analysis of such results in the context of OLR (or spectral OLR) are groundless. The author can define this as a flux quantity, but by no means it is OLR. The author shows a seemingly good agreement between heavily averaged CERES OLR and derived OLR (at SNO or global mean), but this seemingly good agreement can be due to many compensating errors (as I will discuss this in more detail in following comments). This is not something we can argue “end justified the means”, because the “means” here is fundamentally wrong according to the physics, unless the author can approve the otherwise. Note the SNO approach is powerful for comparing radiometric quantities directly measured by the instrument, as shown in many recent calibration studies. But OLR here is not a derive quantity and compensating errors must be identified if the authors want to employ this approach.

We agree that the isotropic assumption is inaccurate to use in this context and we did not make this assumption. We performed the comparison with radiance quantities only, from both IASI and CERES, to avoid adding the uncertainties involved in the flux-to-radiance conversion. We agree that this mistake was easy to make however, as we used the term OLR to stand for Outgoing Longwave Radiance when this acronym is almost always synonymous with the flux quantity. We have rewritten the paper to remove this confusion by using the terms INLR (Integrated Nadir Longwave Radiance) to refer to the broadband radiance product and CINLR (Cloud Integrated Nadir Longwave Radiance) to replace the radiance CRF (Cloud Radiative Forcing) quantity. We have also added a paragraph to the introduction that extensively states this (page 8, line 20 to page 9, line 9). Further we have also removed the sentence in the conclusions which made a crude estimation of the outgoing flux equivalent.

2. **Limitation of A “one-fit-all” regression model for all scene types over the globe** The study employs a regression model to estimate farIR spectral flux after carefully selecting the predictor midIR channels, as shown in Eq. (1). My understanding is Eq. (1) is applied to the entire globe and there is no separate set of parameter derived for different scene types (e.g., ocean vs. land vs. snow surfaces, overcast

vs. partial cloud etc.). It is well known that the regression model works best for the mean state and can behave badly for individual state that is largely deviated from the mean state. This is, in my opinion, why in observations like ERBE or GERB, more physics based angular distribution model approach has been adopted instead of such statistical regression. Physically, different scene types (surface type and cloud properties) can have very different spectral dependence, especially for midIR channels that are sensitive to the surface emission. Therefore, a regression model working best for ocean surface might not work for the land surface, and vice versa. Taking cloud fraction and cloud optical depth into account will further compound this issue exponentially. Even a set of regression coefficients is derived using thousands of observed profiles, there is virtually no discussion how the regression model behaves for different scene types and how the spectral emissivity of difference surface types has been obtained and incorporated into the simulation/training. As long as the predictor channels used in the regress include channels sensitive to surface emissions, and as long as the authors want to discuss any spatial features beyond global average fluxes, the authors are obligated to discuss the regression errors for different scene types, especially the dependence on the surface type and on the cloud fraction and cloud optical depth (or equivalently cloud emissivity).

In fact, though the globally averaged CERES-IASI OLR difference is small, Figure 8 does show that, even after heave average over one month, a large portion of globe still has OLR difference more than ±10 Wm-2. Such big difference is likely attributed to more than one error sources, but oversimplified regression model is definitely a reason and its error contribution needs quantification. The comparisons with CERES OLR beyond the SNO cases are ill defined due to the different stages of diurnal cycle covered by the Terra/Aqua CERES and IASI. However, this cannot be simply attributed as the dominant error sources for Figure 8 when other sources of errors are not quantified at all.

The model is constructed using 3200 soundings which have been shown by past studies to fully capture the wide variability of atmospheric scenes and conditions (text added on page 10, lines 25-28). The stratification of scenes, simulations with built in instrument errors, and expanded regression model form are all refinements that would further improve the performance of technique, however the purpose of this study is to demonstrate the feasibility of this technique, not argue it has reached the optimal stage, which could be

done in future studies. This has been added to the conclusion, page 20, lines 5-13. Furthermore the benefits of more complicated and sophisticated algorithms usually come with the trade-off of limitation, dependencies and possibly additional uncertainties in the auxiliary inputs, while not necessarily guaranteeing better overall accuracy or precision. At this stage we prefer to keep this algorithm self-contained with the IASI radiance observations alone.

We agree that the global composite comparison between IASI and CERES incorporates errors due to sampling differences in time and space which are difficult to separate from errors in the regression algorithm. As advised we have removed section 3.2 and figure 8 entirely.

3. **Title vs. content** The title leaves an impression that this study is to use IASI to estimate spectral flux over the entire LW spectrum (i.e. "the total spectrum of OLR" as in the title). However, the only validation done in this study is comparison with CERES OLR. A good agreement with OLR is necessary condition for a good estimate of the total spectrum of OLR, but not a sufficient condition at all, let alone the quantity derived in this study is not OLR at all (see my comment #1). There are so many possible compensations among different spectral bands that makes the total OLR correct but for utterly wrong reasons. In another word, the question posed in the title has not been convincingly answered by this study at all.

   This study employs a simple and physically incorrect conversion from radiance to flux, as I discussed in comment #1. This conversion alone leads to errors in all spectral channels, midIR and farIR. Then when the summation of spectral flux is computed, it is not clearly at all how much of the agreement with CERES broadband OLR is due to compensations of errors among different channels (or different bands). Even there is no spectrally resolved observations in the farIR that are suitable for direct validation of the algorithm, it seems the study can at least use LBLRTM to simulate farIR spectral flux and IASI radiance simultaneously, then compare the spectral flux regressed from such simulated IASI radiance against the spectral flux computed by LBLRTM directly. Such comparison should be done for clear-sky scenes as well as cloudy-sky scenes with a variety of cloud fractions. Relevant to this issue, the text especially the long introduction reads more like the farIR being the focus of this paper instead of spectral OLR of the LW spectrum. The farIR, as a band, has been discussed more than any spectral details of the flux as computed in this study (which is not the OLR per se)

With the lack of any space borne instruments that isolate the far infrared we cannot evaluate each simulated spectral lines individually. We emphasise the limitations of the model in the conclusions, page 19, line 26 to page 20, line 4. However the broadband comparison is the most independent observational test available, because the algorithm is not constructed with broadband targets but spectral ones, i.e. no broadband observations are involved in the training of the INLR product so there is no reason that compensation would exist to bring the overall values closer together. The fact that the two products are so close in value provides us with confidence in the applicability of this algorithm. We have retitled the paper to *Using IASI to simulate the total spectrum of Outgoing Nadir Longwave Radiance* to emphasise that this is a pilot project that explores the feasibility of this approach, rather than having reached the final stage.

The kind of analysis the reviewer suggests doesn't give new information beyond the limitations of the model, only that the model was constructed correctly. We have added an error analysis to this effect in the methodology, page 11, line 28 to page 12, line 9, and show 2 new figures (Figures 5 and 6), which show the rms errors and the relative rms errors both of which are small. Our study further strengthens the case for a space borne far infrared instrument with which to further validate and develop this model.

The reviewer is right to feel that the far infrared is the focus of this study as, apart from the NIR which contributes very little, this is the only region that was constructed, given that IASI provides direct continuous measurements over the mid infrared region. The spectral resolution of the simulated far infrared region is the main benefit, however the total product constructed is the total outgoing longwave spectrum, which is what allows it to be evaluated against other broadband products. We have clarified the main aim of the paper being to construct the spectrum, and the INLR is used as a tool for its evaluation.

Manuscript prepared for Atmos. Chem. Phys. Discuss.
with version 2014/05/30 6.91 Copernicus papers of the LaTeX class copernicus.cls.
Date: 10 December 2014

~~Can~~ Using IASI ~~be used~~ to Simulate the Total Spectrum of Outgoing Longwave ~~Radiation?~~Radiances

Emma C. Turner[1], Hai-Tien Lee[2], and Simon F. B. Tett[1]

[1]School of Geosciences, University of Edinburgh, UK
[2]Earth System Science Interdisciplinary Center, University of Maryland, College Park, Maryland, USA

Correspondence to: Emma Turner
(et384@cam.ac.uk)

Abstract

A new method of deriving high-resolution top-of-atmosphere spectral radiances in 10181 bands, over the whole outgoing longwave spectrum of the Earth, is presented. ~~Correlations between selected channels of~~ Theoretically derived correlations between channels measured by the Infrared Atmospheric Sounding Interfermeter (IASI) on the MetOp-A satellite and ~~simulated unobserved wavelengths in the far infrared~~ unobserved wavenumbers are used to estimate ~~radiances~~ far infrared radiances at 0.5 cm^{-1} intervals between 25.25 - 644.75 cm^{-1} ~~at 0.5 cm^{-1}intervals. The same method is used in the~~ (the far infrared), and additionally between 2760 - 3000 cm^{-1}. The spectrum is validated by comparing the Integrated Nadir Longwave Radiance (INLR) product (spanning the whole 25.25 - 3000 cm^{-1} ~~region. Total integrated all-sky radiances are validated with~~ range) with the corresponding broadband measurements from the Clouds and the Earth's Radiant Energy System (CERES) instrument on the Terra and Aqua satellites at ~~simultaneous nadir overpasses~~points of simultaneous nadir overpass, revealing mean differences of 0.3 $Wm^{-2}sr^{-1}$ (0.5% relative difference)~~lower for IASI relative to CERES and significantly lower biases in nighttime~~ , this is well within the uncertainties associated with the measurements made by either instruments, however, with noticeable contrast of the biases when separating nighttime and daytime only scenes. ~~Averaged global data over a single month produces mean differences of about 1 $Wm^{-2}sr^{-1}$ in both the all and the clear-sky (1.2% relative difference)~~In the absence of an operational spaceborne instrument that isolates the far infrared this product provides a useful proxy for such measurements, within the limits of the regression model it is based on, which is shown to have very low root mean squared errors. The new high resolution spectrum is presented for global mean clear and ~~total~~ all skies where the far infrared is shown to contribute 44% and 47% to the total ~~OLR respectively, which is~~ INLR respectively, consistent with previous estimates. In terms of ~~spectral cloud radiative forcing~~the spectral cloud effect (CINLR), the FIR contributes 19% and in some subtropical instances appears to be negative, results that would go un-observed with a traditional broadband analysis.

1 Introduction

By lieu of the fact that different thermal wavelengths are sensitive to different atmospheric components, remotely sensed hyperspectral and narrowband radiance measurements contain valuable information about atmospheric, surface and cloud properties, and also reveal fingerprints of long-term climate trends (Harries et al., 2001). Additionally they have a unique value in evaluating climate models (Goody et al., 1998). As such there is a need for detailed and complete satellite observations of terrestrial outgoing longwave radiation (OLR) in the ~~0~~ 25 - 3000 cm^{-1} wavenumber range (3 - 1,000 μm wavelength) at the spectral level (Anderson et al., 2004). At the present time, however, there is no satellite instrument in operation that isolates a substantial part of the OLR with the longest wavelengths, known as the Far Infrared (FIR).

The FIR, which we define as those wavenumbers between ~~0~~ 25 - 650 cm^{-1} (15 - ~~1,000~~ 400 μm), is modulated by water vapour absorption in the pure rotation band and, to a lesser extent, the water vapour continuum. For the all-sky Harries et al. (2008) estimate that about 45% of the total OLR from the Earth is from the FIR. Although individual transitions in this region are low in energy because rotational transitions are lower in characteristic frequency than vibrational transitions, the combined intensity of outgoing radiance at these wavelengths is large and absorption is so strong that over much of the FIR the troposphere is nearly opaque. For this this reason emissions occur mostly in the upper tropospheric and stratospheric regions.

A number of potential uses arise from resolving the FIR with satellite measurements (Mlynczak et al., 2004). Currently retrievals of upper tropospheric water vapour (UTWV) by space-borne instruments exclusively focuses on the vibrational-bending mode (ν_2) which is centred at 1595 cm^{-1} (6.3 μm). However research has shown that the radiance from the rotational mode may be up to 6-7 times more sensitive to water vapour changes than the ν_2 mode (Rizzi et al., 2002; Huang et al., 2007). Harries et al. (2008) estimate the accuracy of of the retrieval performance of the FIR to be comparable to, and sometimes slightly better than, an equivalent mid infrared sounder. Given the disproportionally large role that UTWV has in modulating the Earth's radiation balance relative to the fraction of total atmospheric water it makes up, improving the accuracy with which its vertical distribution is measured would have far-reaching benefits. Additionally, continuum absorption, where the absorption of radiation by water vapour varies smoothly with wavelength is an area that is still not fully understood (Shine et al., 2012) and recent case studies have identified discrepancies in the strength of FIR continuum of up to 50% from estimates based on theory (Green et al., 2012). ~~In a warmer world there will be an increase in water vapour due to its positive feedback~~ Because the relative humidity is expected to remain constant, the water vapour mixing ratio will increase in a warmer world (Soden and Held, 2006). Given that water vapour is the most important atmospheric gas in terms of greenhouse effect (Miskolczi and Mlynczak, 2004), and given that peak greenhouse forcings occur in the far infrared which implies a strong contribution in directing future climate change (Sinha and Harries, 1995), it is vitally important that we increase our understanding of the role of the FIR with global, long-term observations. Particularly as due to its complexity it is unlikely that global climate models get the impact of feedbacks on the FIR under changing climate right (Harries et al., 2008).

Cirrus clouds have a significant effect on the OLR balance as their cold tops essentially shift radiative emission to lower frequencies, with a higher proportion of the OLR coming from the FIR. The amount of emission is strongly connected with the clouds height and temperature structure (Maestri and Rizzi, 2003) so essentially clouds can be characterised by their spectral signatures. Rizzi and Mannozzi (2000) estimate that the ratio of FIR to OLR increases by ~~an average of around~~ approximately 30% from ~~clear to cloudy instantaneous conditions~~a clear scene to a cloudy scene, with stronger effects being seen in ice clouds (Wang et al., 2014; Dessler and Yang, 2003; Mannozzi et al., 1999) . With the recent increase of available global cloud property datasets afforded by the range of instruments on the A-Train satellite group, there is a need to gain corresponding complete descriptions of the clouds in terms of their spectrally resolved radiative properties, including over the FIR.

Current operational space borne hyperspectral sounders such as the Atmospheric Infrared Sounder (AIRS) (Chahine et al., 2006) or the Infrared Atmospheric Sounding Interfermeter (IASI) (Blumstein et al., 2004) have been designed to measure only the mid infrared part of the OLR. Photons at FIR frequencies have lower energies than typical band gap energies so suitable photodiodes are difficult to make. Mercury Cadmium Telluride (HgCdTe) detectors such as those used within the IASI instrument can be designed for lower frequencies, however a 650 cm^{-1} cut off is common due to the enhanced sensitivity required to measure below this threshold. In order to maintain the high signal to noise ratio the detector needs to be cooled significantly to reduce the number of photons generated by the detector itself and achieve the precision required. Microwave satellite detectors such as the Microwave Limb Sounder (MLS) or the Advanced Microwave Sounding Unit (AMSU) sense wavelengths that fall just longer than the FIR, however they use very different radiance measurement technologies. Both of these restrictions from either side of the FIR result in an unmeasured segment of electromagnetic radiation that has generally only been observed as part of the total infrared radiation by broadband devices.

Currently the only spaceborne instrument to spectrally resolve part of the FIR has been the Infrared Interferometer Spectrometer (IRIS) which flew onboard the Nimbus 3 and Nimbus 4 satellites in 1969 and 1970 respectively (Hanel et al., 1972). It had a maximum wavenumber of 400 cm^{-1} (25 μm) and a spectral resolution of 2.8 cm^{-1}. Since then, a limited number of instruments have been developed to measure part of, or all of, the FIR. Some have been part of balloon-borne and ground-based campaigns, such as the Atmospheric Emitted Radiance Interferometer (AERI) (Turner et al., 2004), and the Radiation Explorer in the Far InfraRed (REFIR-BB/PAD) (Esposito et al., 2007), whose measurements have been used to test the representation of the FIR by line-by-line radiative transfer models (Bianchini et al., 2008). Aircraft campaigns using instruments such as the Tropospheric Airborne Fourier Transform Spectrometer (TAFTS) Green et al. (2012), REFIR-PAD (Palchetti et al., 2008), and the Interferometer for Basic Observation of Emitted Spectral Radiance of the Troposphere (I-BEST) Masiello et al. (2012), have been used to gain insights into the FIR continuum. Though these airborne experiments do prove useful for testing parametrisations in radiative transfer models, only spaceborne instruments can give the full Earth coverage of sufficient temporal length needed for climate studies.

Recently, much work has been put into developing and testing a detector proposed for a spaceborne mission with a response in the 50 - 2000 cm^{-1} range at high spectral resolution (approximately 0.643 cm^{-1}). The Far-Infrared Spectroscopy of the Troposphere (FIRST) instrument (Mlynczak et al., 2004) has detectors that are cooled to 4.2K with liquid helium to achieve the necessary sensitivity (for comparison the optical core of IASI is 91.3K). Initial comparisons of FIRST measurements taken on balloon flights against theoretical calculations and spectral overlaps with coincident satellite instruments show excellent fidelity (Mlynczak et al., 2006), however, despite high priority recommendations (see Board et al. (2007)) there is currently no scheduled launch date for its deployment, even though it is often noted that the FIR has been measured extensively and directly on every planet in the solar system except Earth ~~and Pluto~~ (Hanel, 2003).

Historically, when ~~part~~ parts of the infrared spectrum ~~has not been measured~~ are unmeasured from space the remaining bands ~~are~~ have often estimated through alternate means. Previous studies have sought to reproduce total OLR from narrowband and hyperspectral sounders with the combined motivations of validating current operational broadband sounders, mitigating them against potential failure and gaining wider diurnal coverage. The absence of an instrument that measured total outgoing LW flux in the ~~late~~ 1970's led to its estimation using a single waveband in the 800 - 950 cm^{-1} window region (10.5 ~~μm~~ - 12.5μm) from the two-channel scanning radiometer onboard the NOAA-1 ~~-~~ to NOAA-5 satellite platforms via a non-linear regression model derived from radiative transfer calculations applied to 99 different atmospheric profiles (Gruber, 1977; Gruber and Winston, 1978). As the reference broadband results are obtained from a radiative transfer code this method is termed 'theoretical'. Alternatively, Ohring et al. (1984) ~~use~~ used the Earth Radiation Budget (ERB) broadband OLR measurements on the Nimbus 7 satellite as a reference to obtain regression coefficients between these and window band observations from the Temperature Humidity Infrared Radiometer (THIR) instrument on the same satellite at collocated footprints. This method is termed 'empirical', because actual measured data is used as a reference.

~~Clearly, there are uncertainties~~ There are uncertainties involved in using only one ~~spectral region~~ narrow band to estimate the entire OLR ~~. Accordingly, an outgoing LW flux product from the~~ because the atmospheric information contained in one spectral region is limited, eg. see Gruber et al. (1994) . An early theoretical OLR product derived with a multi-spectral regression technique used the 4 infrared channels from the Medium Resolution Infrared Radiometer (MRIR) on the Nimbus-3 satellite (Raschke et al., 1973) . This method has been adapted for use with the High Resolution Infrared Sounder (HIRS) instruments ~~was developed in the 1980's by Ellingson et al. (1989a) using multi-spectral regression between OLR and HIRS radiances simulated from a theoretical radiation model, which explains more than 99% of the significance. This product is useful for its longevity and recent incarnations show~~ that have been operational since 1978, thus providing a continuous longterm surrogate for total OLR (Ellingson et al., 1989a) . The product has been continuously developed since its creation and has demonstrated extremely high correlations with CERES broadband data ~~, with global mean differences less than 2 Wm^{-2}~~ (Lee et al., 2007). Recently, Sun et al. (2010) have used the empirical approach to derive broadband data from AIRS using the CERES outgoing LW flux to generate regression coefficients from principal component ~~scores~~ analysis of AIRS radiances. ~~The AIRS OLR therefore is based empirically on OLR estimates from CERES, and as such mean biases between the two products are low (0.26 Wm^{-2}) .~~

~~As~~ Traditionally, these methods employ data from instruments that fly on polar orbiting satellites which are beneficial for global climate studies in terms of their high spatial coverage. However, as they are restricted to monitoring each subsatellite point just twice a day they fall short of the requirements for diurnal analyses. Geostationary satellites, on the other hand, complete a full Earth scan in approximately 30 minutes thus capturing the daily variability, but are restricted to one nadir location with views at increasingly unfavourable angles away from the subsatellite point. Gube (1982) was the first to use geostationary radiances from the 2 infrared channels (10.2 - 13 μm and 5.7 - 7.5 μm) on the METEOSAT-1 satellite to estimate total OLR flux theoretically. Schmetz and Liu (1988) modified this approach using METEOSAT-2 data to include a better treatment of limb-darkening using the method developed by Abel and Gruber (1979) , and Cheruy et al. (1991) calculated the relationship between METEOSAT-2 data and collocated footprints from broadband Earth Radiation Budget Experiment (ERBE) measurements to produce empirical regression coefficients. The Geostationary Operational Environment Satellite 6 (GOES-6) Imager window channel (10.2 - 12.2 μm) has also been employed in an empirical estimation of OLR fluxes using ERBE data (Minnis et al., 1991) , and Lee et al. (2004) blended HIRS OLR fluxes from polar satellites with GOES-8 Imager data to provide OLR data to incorporate multi-spectral information on temperature and humidity at different elevations, with wider diurnal coverage.

The body of work that exists surrounding the derivation of broadband OLR from narrowband mid infrared measurements is extensive and on-going, however, as regards spectrally resolved measurements in the FIR, progress is limited to a handful of studies. Huang et al. (2006) use clear-sky radiances from the IRIS instrument to predict fluxes in its uncovered spectral regions below 400 cm^{-1} and above 1400 cm^{-1} by assuming a linear relationship between these regions and fluxes in the H_2O ν_2 band and a narrow window region. Regression coefficients between measured and unmeasured wavebands are obtained from calculated radiances using the MODTRAN radiative transfer model applied to simulated profiles from the GFDL AM2 global climate model. These coefficients are then applied to IRIS to simulate the whole OLR. ~~The authors find mean differences of 0.72 Wm^{-2} between IRIS OLR and fluxes produced from ECMWF ERA-40 reanalysis data for the tropical oceans, but noted that when the analysis is broken down by wavelength biases are larger but of opposite signs so compensate overall.~~ Huang et al. (2008) adapt this theoretical method for the hyperspectral Atmospheric Infrared Sounder (AIRS) to derive spectral fluxes in its uncovered wavebands using principle component analysis. A complete set of clear-sky fluxes from 10 to 2000 cm^{-1} are calculated at 10 cm^{-1} intervals, and validated with broadband observations using collocated CERES data ~~. Annual mean differences of 0.67 Wm^{-2} are found over~~ for the tropical oceans~~for 2004. A corresponding analysis for cloudy pixels yields equivalent differences of 2.15 Wm^{-2} (Huang et al., 2010) and similar analyses reveal differences up to 1.73 and 3 Wm^{-2} for the clear and all-sky respectively, depending on the year examined~~ . Corresponding studies were carried out for cloudy data (Huang et al., 2010) , and additional years (Huang et al., 2013). Chen et al. (2013) extend this work to include land and extra-tropical ocean ~~pixels and find global mean differences of 0.96 Wm^{-2} for the daytime, and 0.86 Wm^{-2} for nighttime~~ regions using clear-sky data only.

In lieu of the lack of complete FIR observations we follow ~~the approach taken by previous studies~~ a theoretical approach and develop an algorithm to ’fill in the gaps’ of the available data~~. The high-resolution IASI instrument is used~~, but with a spectral resolution and range of estimated wavenumbers that is an advance on previous studies. To do this we use the IASI instrument which measures in the mid infrared, originally designed to fulfil both meteorology requirements of high spatial coverage, and atmospheric chemistry needs such as accuracy and detailed vertical resolution (Clerbaux et al., 2009). IASI has 4 times as many channels as the AIRS instrument for the same range of thermal infrared wavelengths, and is free from gaps over the whole spectral range. It is part of the payload of the MetOp-A satellite, which provides a differently timed polar orbit and hence a different sampling of the diurnal cycle to existing satellites that carry broadband instruments. In the absence of any current spaceborne instrument that isolate the FIR our new algorithm has the potential to provide valuable proxy measurements, within the limitations of the spectroscopy implemented in the radiative transfer code, that is used to derive the prediction model. To ensure high accuracy we use the Line-By-Line Radiative Transfer Model (LBLRTM) (Clough et al., 1992, 2005) available publicly at http://rtweb.aer.com, which has a long and successful heritage of being at the leading edge of the field, is continually updated and has been well validated, see for example (Shephard et al., 2009; Delamere et al., 2010; Alvarado et al., 2013) .

This study differs from most of its associated predecessors by remaining in the directional radiance regime, with no attempt made to translate unfiltered IASI radiances or the total integrated OLR product to flux densities at this stage. Flux is calculated by integrating the measured radiance over all solid angles, which can be split into zenith and azimuth angles. The outgoing radiation field is strongly anisotropic and must be estimated using a predetermined model, of which many exist involving varying degrees of sophistication and assumptions. These can be either theoretically determined using radiative transfer model calculations of flux or empirically derived using satellite measurements over several different viewing angles and locations, for example see Clerbaux et al. (2003); Loeb et al. (2003); Kato and Loeb (2005) . The resulting Angular Distribution Models (ADMs) relate the radiance measured at a single angle to irradiance estimated over all angles, and as such introduce a further level of uncertainty into the validation, which can be up to 2.3% for recent satellite products (Instantaneous LW TOA flux: see the CERES Terra Edition3A SSF Data Quality Summary). To avoid confusion we use the abbreviation INLR (Integrated Nadir Longwave Radiance) to refer to the extended spectrum of IASI radiances that has been integrated over all wavenumbers, and is distinct from

OLR which is synonymous with the integrated fluxes. This approach has the advantage of allowing for a cleaner comparison with climate model simulated satellite products. The adaption of the methodologies adopted in this study for the additional calculation and evaluation of flux quantities are left for future studies.

We use a theoretical based regression technique similar to the one used to derive OLR from the HIRS instrument based on physical atmospheric profiles which is described in section 2.2. In order to verify the ~~calculated IASI OLR product we perform an independent comparison with broadband~~ extended IASI spectrum we compare the calculated INLR with broadband CERES instruments on other satellites, which avoids the introduction of compounded errors from radiative transfer model evaluations. Section 2.4 explains how times and locations are identified where the path of MetOp-A crosses those of the Aqua and Terra satellites, both of which carry CERES instruments. By restricting this set further to only nadir looking views the instruments will sense the same ~~scene~~ atmospheric path at the same time, providing the opportunity for indirect validation of the new IASI ~~OLR~~ product. Results of this ~~, and a global composite comparison,~~ are presented in section 3.1~~and section **??** respectively~~. Finally the complete constructed ~~OLR~~ IASI spectrum is presented in the remaining sections 4.1, 4.2 and 4.3. ~~In this study no attempt has been made to translate unfiltered IASI radiances to fluxes avoiding the need to involve angular distribution models (ADMs) at this stage. ADMs are empirical relationships between radiances measured at a single angle to irradiance estimated over all angles (Loeb et al., 2003) , and as such introduce a further level of uncertainty into the validation, which can be up to 2.3% (Instantaneous LW TOA flux: see the CERES Terra Edition3A SSF Data Quality Summary). This also allows for a cleaner comparison with climate model simulated satellite products in the future. Therefore, the abbreviation OLR refers to the total LW radiance product herein.~~

2 Data and Methodology

2.1 IASI Level 1c and Combined Sounding Products Data Set

The IASI Flight Model 2 (FM2) instrument is onboard the MetOp-A satellite launched by EUMETSAT in October 2006 which operates in a sun-synchronous orbit. It is a 8461 channel passive sounder that measures in the mid infrared spectral region between 645 - 2760 cm^{-1} (3.62 - 15.5 μm) at a 0.25 cm^{-1} sampling interval with no gaps. The apodised level 1c radiances have a 0.5 cm^{-1} resolution. The effective field of view (EFOV) is a 2 x 2 matrix of 4 circular instantaneous fields of view (IFOV) that each have an approximate footprint diameter of 12 km at nadir. There are 30 EFOV per scan line which takes 8 seconds to complete and had a maximum scan angle of 48.3° in the across track direction. In its nominal mode IASI uses a view of an internal blackbody and deep space once every scanline to calibrate on-board, as described by Simeoni et al. (2004). It is thought to have an average absolute radiometric accuracy of 0.5K, measured in brightness temperature (personal communication with EUMETSAT).

We restrict the data to the IFOVs with the smallest satellite zenith angles in order to retain only nadir looking pixels. There are 4 IFOVs with angles less than 1.5° which are indices 57, 58, 63 and 64 in the across track direction and have viewing angles of 1.34°, 1.37°, 1.41°, and 1.39° respectively. Alongside the level 1c radiances clear-sky flags are obtained from the related level 2 combined sounding products to construct an equivalent clear-sky product. Cloud detection in IASI pixels is performed from a choice of 5 separate tests, involving window channels, AMSU-A, AVHRR and CO_2 slicing, depending on the quality of the input data.

2.2 Method for Estimating ~~OLR~~ Radiances at Unmeasured Wavenumbers from IASI

Strong correlations ~~can be~~ are found between frequencies in the LW spectra with similar spectroscopic properties. Unmeasured radiances with FIR wavenumbers between 25 and 650 cm^{-1} and those between 2760 and 3000 cm^{-1} (which we will term near infrared (NIR) radiances) can be estimated from IASI observations. For example, FIR wavenumbers in the strong H_2O rotational band ~~such as~~ at 25.25 cm^{-1} ~~can~~ have strong correlations with those in the centre of the

667 cm^{-1} CO_2 and 1533 cm^{-1} H_2O ν_2 bands by virtue of their similar sensitivity to high altitude temperatures (Figure 1). However the 1533 cm^{-1} band is physically more similar to frequencies in the FIR and therefore has comparably larger correlations.

Adapting the simulation methodology of Ellingson et al. (1989a), the Line-By-Line Radiative Transfer Model (LBLRTM) ~~(Clough et al., 1992, 2005) available publicly at ,~~ is used to simulate LW spectra over the spectral range 25-3000 cm^{-1} at 0.5 cm^{-1} resolution with radiosonde data from 1600 soundings (Phillips et al., 1988). This dataset was carefully compiled by Dr. Norman Phillips with the purpose of creating a representative sample of the range of conditions found in the atmosphere, and has been demonstrated to be adequate enough to base global models upon, see Ellingson et al. (1989b) . The following details from Ellingson et al. (1989a) describe the dataset. Each sounding includes temperature values at 65 different pressure levels from 0.1 to 1000 mb and mixing ratios of H_2O and O_3 in the corresponding 64 layers. The soundings were compiled from radiosonde ascents from land and ocean stations between 30° S and 60° N and the soundings were equally divided between tropical (30° S - 30° N) and midlatitude (400 summer and 400 winter) conditions. The O_3 data was chosen to be climatologically consistent with the temperature profiles, and the stratospheric H2O mixing ratio is assumed to be 3 ppmm. A second set of cloudy simulations ~~is~~ was obtained by inserting a cloud into each profile at a particular level (randomly distributed) ~~.~~ to give 3200 different conditions, 1600 clear and 1600 cloudy. The water vapour profile was not altered when a cloud layer was included and the clouds were nearly uniformly distributed in low (950 - 850 mb), middle (675 - 525 mb) and high (400 - 240 mb) layers. Clouds are all considered to have 100% horizontal coverage of the profile. Those with cloud top pressures greater than 450 mb are assumed to be spectrally black whereas the high level clouds are assumed to have the spectral properties of cirrus given by Haurwitz and Kuhn (1974) .

Several regression model formulations were investigated for the purpose of NIR/FIR radiance prediction. A log-log transformation was found to provide the optimal performance in minimization of estimation errors and regression residual distributions. This empirical behaviour can also be explained physically, as transmittances vary with optical path via an exponential relationship and hence the model will be approximately linear. Figure 2 shows an example of the log-log relationship between radiances at 33.75 cm^{-1} and the channel that has a maximum correlation with it (2091.25 cm^{-1}).~~Root mean square errors are about 0.4% for all angles.~~

The best predictor channels are selected as those with maximum correlation coefficients between the log-radiances (Figure 3) ~~and the corresponding regression coefficients are found (~~whose values are shown in Figure 4~~)~~. For this application the local zenith angle is restricted to the nadir cases. The prediction equation to estimate the radiance $I_{\nu_{FIR/NIR}}$ in either the FIR or NIR regions at wavenumber ν can be written as,

$$\ln(I_{\nu_{FIR/NIR}}) = a_0 + a_1 \ln(I_{\nu_{predictor}}) \tag{1}$$

where $I_{\nu_{predictor}}$ is the radiance observed by IASI at the predictor wavenumber (Wm^{-2}sr^{-1}(cm^{-1})$^{-1}$) and a_0 and a_1 are the calculated regression coefficients. The mean spectral radiance calculated by LBLRTM for each wavenumber in the FIR is shown in the left panel of Figure 5 and has a total integrated value of 36.32 Wm^{-2}sr^{-1}. The corresponding value for the NIR region is 0.028 Wm^{-2}sr^{-1}. The root mean square (rms) errors in the regression model serves as the theoretical estimates for the modelling uncertainties in the reconstructed spectrum. The right panel of Figure 5 shows these errors for the FIR region. The root mean square of the sum radiance errors, including cancellations from positive and negative values, is 0.054 Wm^{-2}sr^{-1} over all simulated regions which gives a total relative error of 0.15%. Individual root mean square relative errors are shown in Figure 6 which shows a very low dependency on wavenumber.

2.3 CERES Single Scanner Footprint (SSF) Ed3A

The ~~broadband OLR~~ INLR product constructed from the extended IASI radiances is compared with ~~existing~~ the existing CERES directional radiance product. The CERES ~~products. CERES~~ SSF Edition 3A dataset is obtained from the Atmospheric Science Data Center at the NASA Langley Research Center for both the Terra and Aqua polar orbiting satellites (Wielicki et al., 1996). In the cross-track scanning mode there are 90 FOVs in a single scanline ~~that each consist of a circular pixel measuring 20 km diameter at nadir~~with a 25 km footprint at nadir, however in terms of measurements and products it usually considered at a resolution of about 20 km. The swath takes 6.6 seconds to complete and has a maximum scan angle of 65.8°. For the present study only pixels with the minimum satellite zenith angles, which are less than 1° (FOV 45 and 46) are selected to retain only nadir-looking views. Cloud properties for CERES instruments are inferred from the Moderate-Resolution Imaging Spectroradiometer (MODIS) imager which flies on the same satellites, and are based on threshold tests with adjacent channels (Minnis et al., 2004). Each satellite carries 2 identical CERES instruments. For the data acquired, Flight Model 1 (FM1) on Terra and Flight Model 3 (FM3) on Aqua are operational in the cross-track mode.

CERES measures filtered radiances in ~~in~~ terms of physical origin (i.e. thermal or solar), rather than ~~wavelength~~imposing wavelength boundaries, however approximate ~~boundaries~~ ranges for the 3 channels are reflected shortwave (SW) (0.3 - 5 μm), total (0.3 - 200 μm), and window (8 - 12 μm). LW radiation is determined from a weighted combination of measurements from the other channels and hence all emitted thermal radiances that fall within the 0.3 - 200 μm (50 - >3000 cm^{-1}) range are included.

Relative errors due to the process of unfiltering radiances are found to be generally less than 0.2% in the LW (Loeb et al., 2001). The uncertainty in net TOA flux due to absolute calibration uncertainty including the radiance-to-flux conversion is 2% in the SW channel and 1% in the total channel at the 95% confidence level (Priestley et al., 2002). Since nighttime LW radiation is based only on the total channel the uncertainties are essentially the same at 1%. For the daytime combining the uncertainties of the SW channel yields an estimate of around 2.1%, which produces an average daily LW uncertainty of 1.5% (see appendix of Loeb et al. (2009) for the derivation)~~The same percentage value holds for both flux and radiance because they are in a proportional relationship by definition~~. Given that the the present study uses CERES unfiltered radiances only, contributed uncertainties from the radiance-to-flux conversion do not apply, but as these errors are unknown the total level of uncertainty has an upper bound of about 1.5%.

Determining absolute radiometric calibration uncertainty once in-orbit is dependent on a reference instrument and it remains a challenge to achieve a reference traceable to international standards. This is a problem of such critical importance that it led to the formation of an international effort called the Global Space-Based Intercalibration System (GSICS) (Goldberg et al., 2011). The current CERES Edition-3 product established FM1 as the reference to place all the CERES instruments of the same radiometric scale, and as such will contain fewer correction uncertainties. All flight models were corrected for spectral darkening at shorter wavelengths (<1 μm) due to UV exposure which caused degradation in both the SW channel and the shorter wavelength region of the total sensors. Studies that use an edition of CERES prior to Edition 3 will be subject to this error, which overestimates flux by as much as a 0.8% (CERES LW flux daytime for FM1 and FM3: see the CERES Terra and Aqua Edition3A SSF Data Quality Summary). Further refinements for the spectral correction have been proposed for the CERES Edition 4 production (Thomas and Priestley, 2014). This revision is expected to improve the accuracy and stability of CERES data, particularly over the daytime land scenes. The present study uses CERES Edition 3 data and as such, it is important to be aware of the possible errors relating to this version.

~~Overall, each algorithm step in new editions adds its own uncertainty so the estimates quoted above are taken here as lower bounds.~~

2.4 Identifying Simultaneous Nadir Overpasses

Two satellites in sun-synchronous polar orbits with different equatorial crossing times will cross in the polar regions at approximately the same north/south latitude each time. When radiometers from both satellites view the same nadir scene at the same time this is called a simultaneous nadir overpass (SNO). Using SNOs are preferable to comparing composite measurements over the same time period because individual scene differences between cloud and surface properties are avoided. This study uses the database of predicted SNOs provided by the National Calibration Center of NOAA; available at http://ncc.nesdis.noaa.gov/SNO/SNOs//NCC_SNOs_prediction_service.html which makes SNO predictions based on the SGP4 orbital perturbation model (Cao et al., 2004).

Aqua has local equatorial crossing times (LECTs) of 13.30 (ascending) and 01.30 (descending), and Terra has LECTs of 22.30 (ascending) and 10.30 (descending). MetOp-A has an ascending node of 21:30 and a descending node LECT of 09:30. 2012 SNOs between MetOp-A and Aqua, and MetOp-A and Terra, are first filtered following the criteria set out in the methodology of Cao et al. (2005). This specifies that at the SNO: 1) the time difference between nadir pixels is less than 30 seconds and, (2) the distance between nadir pixels is less than the diameter of one footprint. Based on the average of the 20 km CERES pixel and the 12 km IASI pixel this threshold is set to 16 km. This yields approximately 100 SNOs for each satellite pair over the course of a year. Using the predictions the closest matches in terms of time and distance were identified in the satellite data for the most nadir-looking field of views for each instrument. The resulting locations of IASI pixels identified as SNOs are shown in Figure ~~5~~7. By virtue of their different equatorial crossing times MetOp-A and Aqua SNOs all lie around 74° N/S and MetOp-A and Terra SNOs all lie around 81° N/S.~~Unfortunately SNO events for polar orbiters are restricted to the polar regions whose conditions are not representative of the whole planet, however this presents an even stricter test for the algorithm as the radiosonde data from which the line-by-line radiances were calculated were only obtained from tropical and mid-latitude scenes. We estimate the biases for the rest of the globe by additionally performing a composite comparison of OLR products in section ??.~~

3 Validation of INLR at Simultaneous Nadir Overpasses with CERES

3.1 ~~Instantaneous OLR at SNOs~~

For maximum consistency with CERES, IASI ~~OLR~~ INLR radiances are cut off at the 50 cm^{-1} lower wavenumber limit, and integrated over all remaining radiances up to 3000 cm^{-1}. ~~OLR~~ INLR estimates from coincident IASI and CERES pixels generally lie close together, with the majority falling within 2 $Wm^{-2}sr^{-1}$ of each other (Figure ~~6~~8). In general differences will be introduced by the slightly different nadir angles and footprint sizes between CERES and IASI, and the accuracy of the colocations. Absolute values range from 30 to over 80 $Wm^{-2}sr^{-1}$ yet there is no identifiable relationship between scene radiance and bias indicating the IASI algorithm is robust against profile conditions at these latitudes. Nighttime radiances show a slightly higher correlation (0.99) compared with daytime scenes (0.98). Whether the lower daytime correlation originates from errors in the SW channel involved in estimating daytime CERES ~~OLR~~radiances, solar backscatter contamination of either instrument or the increased variability of daytime ~~OLR~~ radiances is beyond the scope of this study.

The same results shown as absolute biases (CERES - IASI) are presented as a time series in Figure ~~7~~9, revealing no dependency of error upon season. Table 1 breaks down these biases by CERES instrument. Mean IASI ~~OLR~~ INLR values are about 0.3 $\mathrm{Wm^{-2}sr^{-1}}$ lower than CERES when all local times are considered, and individual differences are generally within ±6 $\mathrm{Wm^{-2}sr^{-1}}$. Larger biases appear to be associated with partly cloudy or overcast scenes and are likely due to horizontal cloud inhomogeneity in the region of the SNO which can have a large effect on the height, and hence temperature/radiance of emission.

When relative differences are considered this corresponds to LW radiances that are 0.5% higher in CERES than IASI. Split into day and nightime scenes it is apparent that this bias is dominated by daytime pixels as the mean nighttime relative error is only 0.01% whereas daytime differences are 0.95%. This could be related to the CERES Ed4 findings about the SRF correction determination method. All relative differences are well within the uncertainty range of CERES unfiltered radiance based on absolute radiometric calibration uncertainty and relative unfiltering errors as detailed in section 2.3. Given that the original correlation co-efficients between radiances were calculated using only tropical and mid-latitude profiles, the fact that the algorithm performs so well in polar regions shows that it is highly robust under different scene types.

3.1 ~~Global composite OLR~~

~~In order to obtain an estimate of the magnitude of extra-polar biases, gridded and averaged nadir data from CERES (Aqua and Terra) for the whole month of April 2012 is compared with the equivalent constructed OLR composite from IASI (Figure 8). For a single day there are approximately 40,000 pixels collected for each instrument, binned to a 2.5° x 2.5° grid. Global mean biases split into day and night time scenes along with the differences between Aqua and Terra are also shown in Table ??.~~

~~The IASI OLR product continues to be underestimated with respect to CERES when the whole globe is averaged together, with a bias that is about 3 times greater than the SNO mean bias for both Aqua and Terra (0.79 and 1.04 Wm^{-2}sr^{-1}, with a relative error of 0.94 and 1.26% respectively) in the all-sky. This increase is not wholly unexpected due to the nature of the compositing process and it is likely to be dominated by diurnal variations, which is evident from the general noisiness of the data in Figure 8. More extreme differences can be seen over land and deep cloud regions where diurnal variations are greatest. Dealing with clear-sky pixels only removes the cloudy part of this diurnal variation. On a daily basis clear-sky is identified in 15% of the data, but when gridded and averaged over the month 70% of the globe has clear-sky data. As CERES and IASI use different methods to detect clouds it is possible that they would interpret the cloudiness of the same scene differently thus incorporating a possible systematic bias into the clear-sky comparisons, which are all observed to be higher than their all-sky equivalents.~~

~~The difference due to the 3 hour local time difference between Terra and Aqua (0.26 Wm^{-2}sr^{-1} in the all-sky) indicates time sampling issues are not relatively significant, though a longer time period would undoubtedly reveal clearer patterns. Data volume issues prohibit testing this currently. As with the SNO comparison biases between OLR products are significantly larger in the daytime which falls in line with the existing correction error identified in the Ed3 CERES data mentioned in section 2.3. However, with the exception of daytime clear-sky differences between Aqua CERES and IASI, relative mean biases are still within the uncertainty ranges estimated for CERES for all time periods and given the uncontrollable factors involved in the composite process this gives us confidence that the algorithm used to estimate IASI OLR is spatially robust.~~

4 ~~Spectral~~ Extended IASI ~~OLR~~Spectral Nadir Radiances

4.1 Instantaneous ~~spectral IASI OLR~~Spectrum

Example ~~instantaneous IASI OLR spectra~~ extended instantaneous IASI radiance spectra from 17th April 2012 show that the estimated FIR contributes between ~~43~~ 42 - 64% to the total ~~OLR~~ INLR depending on the scene type (Figure ~~9~~10). This is within the range of previous estimates (Harries et al., 2008). We present night time scenes which is when the FIR is particularly dominant as temperatures fall. In the daytime, however, higher surface temperatures often allow the window region to reach higher intensities when there is little or no cloud (Lindfors et al., 2011) . In non-cloudy cases temperature is the dominating factor controlling the total intensity of LW radiance received at the TOA. For example, the spectrum over the Sahara (Figure ~~9~~10c) emits about double the total radiance as that over Antarctica (Figure ~~9~~10d). However when clouds are present their height and coverage can have a highly significant influence. For example it is certain that the temperature in the tropics will be higher than that in Antarctica, and yet Figure ~~9~~10a and Figure ~~9~~10d have similar values of total ~~OLR~~INLR. This is because it is likely that deep convective cloud brings the height of tropical emission to the cold upper troposphere where photons have lower energies. Clouds give more weight to the FIR as part of the ~~OLR overall, the tropics and the desert~~ INLR overall. The desert and the tropics are both warm regions and yet the FIR contributes ~~43% to the~~ 42% of the former clear dry case and 62% ~~to the~~ of the latter moist cloudy case, which is almost a third greater. ~~Lower~~ The low stratiform clouds that are prevalent over midlatitude land will not have as large an effect on the whole spectrum (Figure 10b), but emission in the window region is still reduced with respect to the FIR~~(Figure 9b) with a higher percentage coming from the FIR (49%) than in the clear-sky desert~~.

4.2 Mean ~~clear~~ Clear and ~~cloudy spectral IASI OLR~~Cloudy Spectrum

When split into global mean clear and cloudy scenes an average of 47% of the total LW radiance comes from wavenumbers less than 645 cm^{-1} when clouds are ~~always~~ present, and 44% when the atmospheric column is clear (Figure ~~10~~11a). The peak wavelength of emission also shifts from 558.25 to 513.25 cm^{-1} in the cloudy only case. The NIR region constructed from a similar method contributes near-negligible radiances of 0.03 Wm^{-2}sr^{-1} (0.04%) in cloudy cases and 0.05 Wm^{-2}sr^{-1} (0.06%) in clear cases. This is a region of partial transparency and hence like the 800 - 1250 cm^{-1} window dominates more in the clear-sky.

The difference between the averaged clear and all-sky is equivalent to the ~~effect of a cloud and~~ cloud effect and using flux quantities this is often know as the cloud radiative forcing (CRF) or the cloud radiative effect (CRE). ~~Figure 10b shows CRF~~ By analogy we use the term ‘Cloud Integrated Nadir Longwave Radiance’ (CINLR) to refer to the radiance equivalent of CRF. Figure 11b shows CINLR values for the whole LW spectrum, with a total value of 8.1 Wm^{-2}sr^{-1} ~~Note that our definition of CRF is in terms of radiance, not flux.~~ In general there is more outgoing radiation at all wavenumbers in the clear-sky because liquid clouds are nearly opaque to the whole ~~OLR~~ infrared radiance spectrum and re-emit at lower temperatures/energies than the clear-sky case. Wavebands at 0 - 200 cm^{-1}, 650 - 700 cm^{-1}, and around 1500 cm^{-1}, are strongly sensitive to rotational water vapour transitions, CO_2 ν_2 transitions, and the vibrational ν_2 water vapour transitions respectively~~, and as~~. As such peak emissions are in the upper troposphere/lower stratosphere where clouds are few and hence the ~~CRF~~ CINLR is low. Even though in the cloudy case the FIR represents a more significant proportion of the total ~~OLR~~INLR, the clear-sky still emits more over this wavelength range in terms of absolute magnitude. Although the majority ~~energy in cloud radiative forcing are~~ of the energy in the CINLR is distributed over the atmospheric window spectral interval, the FIR still accounts for 19% of the total ~~CRF~~CINLR.

4.3 Maps of ~~OLR~~INLR, FIR and window wavebands

Spatially, all-sky IASI ~~OLR~~ INLR averaged over the whole month of April 2012 peaks in the clear desert and extra-tropical subsidence regions around $\pm 20°$. In the latter low maritime clouds emit radiation at high temperatures similar to those at the surface (Figure ~~11~~12a). Deep convective clouds over the intertropical convergence zone, Indo-Pacific warm pool and monsoon regions of Africa and South America reduce ~~OLR~~ INLR because emission is from high, cold cirrus cloud tops. Correspondingly these regions also have the highest ~~CRF~~ CINLR values (Figure ~~11~~12b), as the difference between the all and the clear-sky is at a maximum. An unexpected feature of this plot are occasional negative ~~CRF~~ CINLR values, bordering the polar continents. These values tend not to be lower than -1 $Wm^{-2}sr^{-1}$. ~~CRF~~ CINLR is generally a positive quantity, i.e. if a cold cloud is added to any particular clear-sky scene instantaneously the radiation emitted from the top of the cloud will be reduced with respect to the clear-sky amount. However, when a lower tropospheric temperature inversion is present, clouds can be warmer than the surface. These clouds are particularly common over the Antarctic Plateau in austral winter as a result of the snow-surface emissivity being greater than the atmospheric emissivity. Additionally cloud detection algorithms often struggle in the polar regions due to lack of thermal contrast between ice covered surfaces and cloud tops. Temperature inversions are also a prominent feature of the subtropical trade wind regimes due to adiabatic compression of subsiding warm air masses which produce shallow cumulus clouds that are warmer than the surface. Examples of this behaviour are visible in the data around $\pm 20^\circ$ in Figure ~~11~~12b.

The proportion of the ~~OLR~~ radiance spectrum that falls within the FIR waveband peaks in the coldest latitudes of Antarctica as most of the outgoing photons have very low energies and hence low wavenumbers (Figure ~~11~~12c). It is also higher in regions of greater cloud cover, and this can be identified in the deep convective cloud regions with respect to the surrounding clearer areas, such as over the Sahara. The FIR and the window (WIN) waveband between 800 and 1250 cm^{-1} (Figure ~~11~~12e) are inverse to one another in terms zonal variability, i.e. when the FIR contribution is higher the WIN contribution is lower and vice versa. However, the FIR contributes an average of 40% more to the ~~OLR~~ INLR overall in terms of absolute magnitude. In terms of contribution to the ~~CRF~~ CINLR though, the WIN is 3 times greater on average than the FIR (Figure ~~11~~12d and f), but again the patterns of zonal variability are inverse to each other. ~~Interesting~~Interestingly, in the subtropical subsidence regions there are some negative values of ~~CRF~~ CINLR in the FIR, meaning the average all-sky radiation is more than the average clear-sky at these wavenumbers. As the total ~~OLR~~ INLR and the WIN ~~CRF~~ CINLR are still positive in (most of) these locations these cannot be attributed solely to temperature inversions. It is possible to speculate about the cause of this behaviour, for example, clear skies associated with humid conditions and trade wind inversion clouds associated with dryer conditions would result in a higher emission level for the FIR. It could also be the case that the FIR is more sensitive to a false diagnosis of a cloudy sky pixel as clear than the whole ~~OLR~~ spectrum overall. As a result of these negative FIR ~~CRFs~~CINLRs, the corresponding positive WIN ~~CRFs~~ CINLRs peak at these locations because they are now contributing more to the positive total ~~OLR CRF~~INLR CINLR. This value is still low due these ~~2~~ two parts of the spectrum cancelling with one another, something that would go un-observed with a purely broadband analysis.

5 Conclusions and Discussion

In this study we have shown that IASI can be used to simulate the entire range of wavenumbers (25 - 3000 cm^{-1}) needed to estimate the total ~~outgoing longwave radiation~~ spectrum of outgoing longwave radiances at a sampling resolution of 0.5 cm^{-1} in the far infrared (<645 cm^{-1}) and the near infrared (>2600 cm^{-1}). The method is based on theoretical correlations between measured and un-measured parts of the spectrum, derived using simulations from the line-by-line radiative transfer code LBLRTM applied to 3200 measured atmospheric profiles~~, and is independently verified by broadband instruments on other satellites. Coincident~~ . Broadband observations on other satellite platforms place constraints on the total radiant energy which effectively provides a direct comparison of the simulated regions, assuming the parts of the spectrum where CERES overlaps with IASI are fully in agreement, within the bounds of uncertainty introduced by calibration differences and other factors. This uncertainty is quantified at an upper limit of 1.5% for LW CERES radiances, and coincident all-sky measurements between IASI and CERES at simultaneous nadir overpasses in polar regions show mean differences of about 0.3 Wm^{-2}sr^{-1} (0.5% relative difference), ~~and a composite comparison of all regions gives global mean differences of about 1 Wm^{-2}sr^{-1} (just over 1%) over a single month for all-sky measurements. This is within the 1.5% absolute calibration uncertainty for LW CERES radiances, which is good considering the limited time period. When estimating the difference in units of flux a simple isotropic assumption (flux = π*radiance) yields biases of 0.9~~ which is well within this range. This is a strict test of the regression model, given that the two sets of measurements are completely independent and ~~3.1 Wm^{-2} for the colocated and composite~~

~~analysis respectively, which are comparable in magnitude to those presented in previous studies of all-sky OLR that are constructed in a similar manner. Given that this study uses completely independent measurements from different instruments on different satellites, and~~ approximately 50% of the ~~spectrum~~ INLR is being estimated~~from our method, this is a promising result~~.

Instantaneous examples of the simulated spectrum show the far infrared contributes between 43 - 64% to the total ~~OLR~~ INLR with a global weighted average of 47% in the all-sky and 44% in the clear-sky. The results of our comparison are consistent with previous values proposed in the literature (45% for the all-sky) Harries et al. (2008). This study serves as a proof of concept of the usefulness of IASI for estimating the ~~total LW radiance and the~~ terrestrial far infrared at an unprecedented level of spectral resolution. Quantities such as ~~CRF~~ cloud radiative forcing which are commonly studied only as a single integrated quantity across the ~~OLR~~ longwave spectrum contain much more information when examined on a spectral level~~.~~, and in the absence of any corresponding empirical data in the FIR region this product provides a ‘next best’ alternative. Application of the reconstructed FIR to studies of cirrus clouds has not been explored here, due to the limited knowledge of the spectroscopy and optical properties of these types of clouds which is inherent in the LBLRTM model. This study strengthens the case for a spaceborne far infrared instrument with which to further validate and develop this model on a spectral level.

It is feasible that this product could be developed by applying ~~empirical~~ angular distribution models to the radiances to give flux estimates using a similar approach taken by previous studies (e.g. Huang et al. (2008)), and as such IASI has the potential to be ~~supplementary to the~~ supplement existing broadband instrument observations. The algorithm as it stands is self-contained for all scene types, however, as anisotropy varies considerably with scene the regression algorithm could be customised to consider cloud cover, surface type and further inhomogeneities. Other inclusions in the construction of the model, such as instrument noise and determination of the optimal spectral interval size for the predictors could additionally refine the models performance further in the future. Given that IASI will eventually be carried by 3 different MetOp satellites in the same local-time orbit, and ~~IASI-New~~ IASI - New Generation proposed for the second generation of MetOp satellites will have even higher sampling resolution (0.125 cm^{-1}) (Crevoisier et al., 2013), this provides the possibility of a product with valuable length and the ability to be inter-satellite calibrated between instruments.

Acknowledgements. CERES and IASI data was provided by ~~NASA and EUMETSAT~~ NOAA and EUMETSAT respectively. We thank Norman Loeb and 3 anonymous reviewers for valuable comments. This work was funded as part of ~~a~~ Emma Turner's PhD scholarship by the National Environmental Research Council of the UK.

References

Abel, P. and Gruber, A.: An Improved Model for the Calculation of Longwave Flux at 11 [mu] m, NOAA Tech. Rep. NESS, p. 24, 1979.

Alvarado, M., Payne, V., Mlawer, E., Uymin, G., Shephard, M., Cady-Pereira, K., Delamere, J., and Moncet, J.: Performance of the Line-By-Line Radiative Transfer Model (LBLRTM) for temperature, water vapor, and trace gas retrievals: recent updates evaluated with IASI case studies, Atmos. Chem. Phys, 13, 6687–6711, 2013.

Anderson, J., Dykema, J., Goody, R., Hu, H., and Kirk-Davidoff, D.: Absolute, spectrally-resolved, thermal radiance: a benchmark for climate monitoring from space, Journal of Quantitative Spectroscopy and Radiative Transfer, 85, 367–383, 2004.

Bianchini, G., Carli, B., Cortesi, U., Del Bianco, S., Gai, M., and Palchetti, L.: Test of far-infrared atmospheric spectroscopy using wide-band balloon-borne measurements of the upwelling radiance, Journal of Quantitative Spectroscopy and Radiative Transfer, 109, 1030–1042, 2008.

Blumstein, D., Chalon, G., Carlier, T., Buil, C., Hebert, P., Maciaszek, T., Ponce, G., Phulpin, T., Tournier, B., Simeoni, D., et al.: IASI instrument: Technical overview and measured performances, in: Optical Science and Technology, the SPIE 49th Annual Meeting, pp. 196–207, International Society for Optics and Photonics, 2004.

Board, S. S. et al.: Earth science and applications from space: National imperatives for the next decade and beyond, National Academies Press, 2007.

Cao, C., Weinreb, M., and Xu, H.: Predicting simultaneous nadir overpasses among polar-orbiting meteorological satellites for the intersatellite calibration of radiometers, Journal of Atmospheric and Oceanic Technology, 21, 537–542, 2004.

Cao, C., Ciren, P., Goldberg, M., and Weng, F.: Intersatellite calibration of HIRS from 1980 to 2003 using the simultaneous nadir overpass (SNO) method for improved consistency and quality of climate data, in: Int. TOVS Study Conf, 2005.

Chahine, M. T., Pagano, T. S., Aumann, H. H., Atlas, R., Barnet, C., Blaisdell, J., Chen, L., Divakarla, M., Fetzer, E. J., Goldberg, M., et al.: AIRS: Improving weather forecasting and providing new data on greenhouse gases., Bulletin of the American Meteorological Society, 87, 2006.

Chen, X., Huang, X., Loeb, N. G., and Wei, H.: Comparisons of Clear-Sky Outgoing Far-IR Flux Infered from Satellite Observations and Computed from the Three Most Recent Reanalysis Products, Journal of Climate, 26, 478–494, 2013.

Cheruy, F., Kandel, R., and Duvel, J.: Outgoing longwave radiation and its diurnal variation from combined ERBE and Meteosat observations: 1. Estimating OLR from Meteosat data, Journal of Geophysical Research: Atmospheres (1984–2012), 96, 22 611–22 622, 1991.

Clerbaux, C., Boynard, A., Clarisse, L., George, M., Hadji-Lazaro, J., Herbin, H., Hurtmans, D., Pommier, M., Razavi, A., Turquety, S., et al.: Monitoring of atmospheric composition using the thermal infrared IASI/MetOp sounder, Atmospheric Chemistry and Physics, 9, 6041–6054, 2009.

Clerbaux, N., Dewitte, S., Gonzalez, L., Bertrand, C., Nicula, B., and Ipe, A.: Outgoing longwave flux estimation: Improvement of angular modelling using spectral information, Remote Sensing of Environment, 85, 389–395, 2003.

Clough, S., Shephard, M., Mlawer, E., Delamere, J., Iacono, M., Cady-Pereira, K., Boukabara, S., and Brown, P.: Atmospheric radiative transfer modeling: A summary of the AER codes, Journal of Quantitative Spectroscopy and Radiative Transfer, 91, 233–244, 2005.

Clough, S. A., Iacono, M. J., and Moncet, J.-L.: Line-by-line calculations of atmospheric fluxes and cooling rates: Application to water vapor, Journal of Geophysical Research: Atmospheres (1984–2012), 97, 15 761–15 785, 1992.

Crevoisier, C., Clerbaux, C., Guidard, V., Phulpin, T., Armante, R., Barret, B., Camy-Peyret, C., Chaboureau, J.-P., Coheur, P.-F., Crépeau, L., et al.: Towards IASI-New Generation (IASI-NG): impact of improved spectral resolution and radiometric noise on the retrieval of thermodynamic, chemistry and climate variables, Atmospheric Measurement Techniques Discussions, 6, 11 215–11 277, 2013.

Delamere, J., Clough, S., Payne, V., Mlawer, E., Turner, D., and Gamache, R.: A far-infrared radiative closure study in the Arctic: Application to water vapor, Journal of Geophysical Research: Atmospheres (1984–2010), 115, 2010.

Dessler, A. and Yang, P.: The distribution of tropical thin cirrus clouds inferred from Terra MODIS data, Journal of climate, 16, 1241–1247, 2003.

Ellingson, R. G., Lee, H.-T., Yanuk, D. J., and Gruber, A.: A technique for estimating outgoing longwave radiation from HIRS radiance observations, Journal of Atmospheric and Oceanic Technology, 6, 706–711, 1989a.

Ellingson, R. G., Yanuk, D. J., and Gruber, A.: Effects of the choice of meteorological data on a radiation model simulation of the NOAA technique for estimating outgoing longwave radiation from satellite radiance observations, Journal of climate, 2, 761–765, 1989b.

Esposito, F., Grieco, G., Leone, L., Restieri, R., Serio, C., Bianchini, G., Palchetti, L., Pellegrini, M., Cuomo, V., Masiello, G., et al.: REFIR/BB initial observations in the water vapour rotational band: Results from a field campaign, Journal of Quantitative Spectroscopy and Radiative Transfer, 103, 524–535, 2007.

Goldberg, M., Ohring, G., Butler, J., Cao, C., Datla, R., Doelling, D., Gärtner, V., Hewison, T., Iacovazzi, B., Kim, D., et al.: The Global Space-Based Inter-Calibration System., Bulletin of the American Meteorological Society, 92, 2011.

Goody, R., Anderson, J., and North, G.: Testing climate models: An approach, Bulletin of the American Meteorological Society, 79, 2541–2549, 1998.

Green, P. D., Newman, S. M., Beeby, R. J., Murray, J. E., Pickering, J. C., and Harries, J. E.: Recent advances in measurement of the water vapour continuum in the far-infrared spectral region, Philosophical Transactions of the Royal Society A: Mathematical, Physical and Engineering Sciences, 370, 2637–2655, 2012.

Gruber, A.: Determination of the earth-atmosphere radiation budget from NOAA satellite data, Unknown, 1, 1977.

Gruber, A. and Winston, J.: Earth-atmosphere radiative heating based on NOAA scanning radiometer measurements, Bulletin of the American Meteorological Society, 59, 1570–1573, 1978.

Gruber, A., Ellingson, R., Ardanuy, P., Weiss, M., Yang, S., and Oh, S. N.: A comparison of ERBE and AVHRR longwave flux estimates, Bulletin of the American Meteorological Society, 75, 2115–2130, 1994.

Gube, M.: Radiation Budget Parameters at the Top of the Earth's Atmosphere from METEOSAT Data, Journal of Applied Meteorology, 21, 1907–1921, 1982.

Hanel, R. A., C. B. J. J. D. E. . S. R. E.: Exploration of the Solar System by Infrared Remote Sensing, Cambridge Univ. Press, 2003.

Hanel, R., Conrath, B., Kunde, V., Prabhakara, C., Revah, I., Salomonson, V., and Wolford, G.: The Nimbus 4 infrared spectroscopy experiment: 1. Calibrated thermal emission spectra, Journal of Geophysical Research, 77, 2629–2641, 1972.

Harries, J., Carli, B., Rizzi, R., Serio, C., Mlynczak, M., Palchetti, L., Maestri, T., Brindley, H., and Masiello, G.: The far-infrared earth, Reviews of Geophysics, 46, RG4004, 2008.

Harries, J. E., Brindley, H. E., Sagoo, P. J., and Bantges, R. J.: Increases in greenhouse forcing inferred from the outgoing longwave radiation spectra of the Earth in 1970 and 1997, Nature, 410, 355–357, 2001.

Haurwitz, F. and Kuhn, W. R.: The distribution of tropospheric planetary radiation in the Southern Hemisphere, Journal of Applied Meteorology, 13, 417–429, 1974.

Huang, X., Ramaswamy, V., and Schwarzkopf, M. D.: Quantification of the source of errors in AM2 simulated tropical clear-sky outgoing longwave radiation, Journal of Geophysical Research: Atmospheres (1984–2012), 111, 2006.

Huang, X., Yang, W., Loeb, N. G., and Ramaswamy, V.: Spectrally resolved fluxes derived from collocated AIRS and CERES measurements and their application in model evaluation: Clear sky over the tropical oceans, Journal of Geophysical Research: Atmospheres (1984–2012), 113, 2008.

Huang, X., Loeb, N., and Yang, W.: Spectrally resolved fluxes derived from collocated AIRS and CERES measurements and their application in model evaluation: 2. Cloudy sky and band-by-band cloud radiative forcing over the tropical oceans, Journal of Geophysical Research, 115, D21 101, 2010.

Huang, X., Cole, J. N., He, F., Potter, G. L., Oreopoulos, L., Lee, D., Suarez, M., and Loeb, N. G.: Longwave Band-By-Band Cloud Radiative Effect and Its Application in GCM Evaluation, Journal of Climate, 26, 450–467, 2013.

Huang, Y., Ramaswamy, V., and Soden, B.: An investigation of the sensitivity of the clear-sky outgoing longwave radiation to atmospheric temperature and water vapor, Journal of geophysical research, 112, D05 104, 2007.

Kato, S. and Loeb, N. G.: Top-of-atmosphere shortwave broadband observed radiance and estimated irradiance over polar regions from Clouds and the Earth's Radiant Energy System (CERES) instruments on Terra, Journal of Geophysical Research: Atmospheres (1984–2012), 110, 2005.

Lee, H., Gruber, A., Ellingson, R., and Laszlo, I.: Development of the HIRS outgoing longwave radiation climate dataset, Journal of Atmospheric and Oceanic Technology, 24, 2029–2047, 2007.

Lee, H.-T., Heidinger, A., Gruber, A., and Ellingson, R. G.: The HIRS outgoing longwave radiation product from hybrid polar and geosynchronous satellite observations, Advances in Space Research, 33, 1120–1124, 2004.

Lindfors, A. V., Mackenzie, I. A., Tett, S. F., and Shi, L.: Climatological diurnal cycles in clear-sky brightness temperatures from the High-Resolution Infrared Radiation Sounder (HIRS), Journal of Atmospheric and Oceanic Technology, 28, 1199–1205, 2011.

Loeb, N., Wielicki, B., Doelling, D., Smith, G., Keyes, D., Kato, S., Manalo-Smith, N., and Wong, T.: Toward optimal closure of the Earth's top-of-atmosphere radiation budget, Journal of Climate, 22, 748–766, 2009.

Loeb, N. G., Priestley, K. J., Kratz, D. P., Geier, E. B., Green, R. N., Wielicki, B. A., Hinton, P. O., and Nolan, S. K.: Determination of unfiltered radiances from the Clouds and the Earth's Radiant Energy System instrument, Journal of Applied Meteorology, 40, 822–835, 2001.

Loeb, N. G., Manalo-Smith, N., Kato, S., Miller, W. F., Gupta, S. K., Minnis, P., and Wielicki, B. A.: Angular Distribution Models for Top of Atmosphere Radiative Flux Estimation from the Clouds and the Earths Radiant Energy System Instrument on the Tropical Rainfall Measuring Mission Satellite. Part I Methodology., Journal of applied meteorology, 42, 2003.

Maestri, T. and Rizzi, R.: A study of infrared diabatic forcing of ice clouds in the tropical atmosphere, Journal of geophysical research, 108, 4139, 2003.

Mannozzi, L., Di Giuseppe, F., and Rizzi, R.: Cirrus cloud optical properties in far infrared, Physics and Chemistry of the Earth, Part B: Hydrology, Oceans and Atmosphere, 24, 269–273, 1999.

Masiello, G., Serio, C., Esposito, F., and Palchetti, L.: Validation of line and continuum spectroscopic parameters with measurements of atmospheric emitted spectral radiance from far to mid infrared wave number range, Journal of Quantitative Spectroscopy and Radiative Transfer, 113, 1286–1299, 2012.

Minnis, P., Young, D. F., and Harrison, E. F.: Examination of the relationship between outgoing infrared window and total longwave fluxes using satellite data, Journal of climate, 4, 1114–1133, 1991.

Minnis, P., Young, D. F., Sun-Mack, S., Heck, P. W., Doelling, D. R., and Trepte, Q. Z.: CERES cloud property retrievals from imagers on TRMM, Terra, and Aqua, in: Remote Sensing, pp. 37–48, International Society for Optics and Photonics, 2004.

Miskolczi, F. M. and Mlynczak, M. G.: The greenhouse effect and the spectral decomposition of the clear-sky terrestrial radiation, Quarterly Journal of the Hungarian Meteorological Service, 108, 209–251, 2004.

Mlynczak, M., Johnson, D., Bingham, G., Jucks, K., Traub, W., Gordley, L., and Harries, J.: The far-infrared spectroscopy of the troposphere (FIRST) project, in: Proc. SPIE, vol. 5659, pp. 81–87, 2004.

Mlynczak, M., Johnson, D., Latvakoski, H., Jucks, K., Watson, M., Kratz, D., Bingham, G., Traub, W., Wellard, S., Hyde, C., et al.: First light from the Far-Infrared Spectroscopy of the Troposphere (FIRST) instrument, Geophysical research letters, 33, L07 704, 2006.

Ohring, G., Gruber, A., and Ellingson, R.: Satellite determinations of the relationship between total longwave radiation flux and infrared window radiance, Journal of climate and applied meteorology, 23, 416–425, 1984.

Palchetti, L., Bianchini, G., Carli, B., Cortesi, U., and Bianco, S. D.: Measurement of the water vapour vertical profile and of the Earth's outgoing far infrared flux, Atmospheric Chemistry and Physics, 8, 2885–2894, 2008.

Phillips, N., Susskind, J., and McMillin, L.: Results of a joint NOAA/NASA sounder simulation study, Journal of Atmospheric and Oceanic Technology, 5, 44–56, 1988.

Priestley, K., Wielicki, B., Green, R., Haeffelin, M., Lee, R., and Loeb, N.: Early radiometric validation results of the CERES Flight Model 1 and 2 instruments onboard NASA'S Terra Spacecraft, Advances in Space Research, 30, 2371–2376, 2002.

Raschke, E., Vonder Haar, T. H., Bandeen, W. R., and Pasternak, M.: The Annual Radiation Balance of the Earth-Atmosphere System During 1969-70 from Nimbus 3 Measurements., Journal of Atmospheric Sciences, 30, 341–364, 1973.

Rizzi, R. and Mannozzi, L.: Preliminary results on the planetary emission between 100 and 600 cm -1, REFIR Radiation Explorer in the Far Infrared Final Rep ENV4 CT6, 344, 77–88, 2000.

Rizzi, R., Serio, C., and Amorati, R.: Sensitivity of broadband and spectral measurements of outgoing radiance to changes in water vapor content, in: International Symposium on Optical Science and Technology, pp. 181–190, International Society for Optics and Photonics, 2002.

Schmetz, J. and Liu, Q.: Outgoing longwave radiation and its diurnal variation at regional scales derived from Meteosat, Journal of Geophysical Research: Atmospheres (1984–2012), 93, 11 192–11 204, 1988.

Shephard, M., Clough, S., Payne, V., Smith, W., Kireev, S., and Cady-Pereira, K.: Performance of the line-by-line radiative transfer model (LBLRTM) for temperature and species retrievals: IASI case studies from JAIVEx, Atmospheric Chemistry and Physics, 9, 7397–7417, 2009.

Shine, K. P., Ptashnik, I. V., and Rädel, G.: The water vapour continuum: brief history and recent developments, Surveys in geophysics, 33, 535–555, 2012.

Simeoni, D., Astruc, P., Miras, D., Alis, C., Andreis, O., Scheidel, D., Degrelle, C., Nicol, P., Bailly, B., Guiard, P., et al.: Design and development of IASI instrument, in: Optical Science and Technology, the SPIE 49th Annual Meeting, pp. 208–219, International Society for Optics and Photonics, 2004.

Sinha, A. and Harries, J. E.: Water vapour and greenhouse trapping: The role of far infrared absorption, Geophysical research letters, 22, 2147–2150, 1995.

Soden, B. and Held, I.: An assessment of climate feedbacks in coupled ocean-atmosphere models, Journal of Climate, 19, 3354–3360, 2006.

Sun, F., Goldberg, M. D., Liu, X., and Bates, J. J.: Estimation of outgoing longwave radiation from Atmospheric Infrared Sounder radiance measurements, Journal of Geophysical Research: Atmospheres (1984–2012), 115, 2010.

Thomas, S. and Priestley, K.: CERES FM1 - FM6 Instrument Update., Spring 2014 CERES Science Team Meeting. April 22-24. Hampton, VA, 2014.

Turner, D. D., Tobin, D., Clough, S. A., Brown, P. D., Ellingson, R. G., Mlawer, E. J., Knuteson, R. O., Revercomb, H. E., Shippert, T. R., Smith, W. L., et al.: The QME AERI LBLRTM: A closure experiment for downwelling high spectral resolution infrared radiance., Journal of the atmospheric sciences, 61, 2004.

Wang, C., Yang, P., Dessler, A., Baum, B. A., and Hu, Y.: Estimation of the cirrus cloud scattering phase function from satellite observations, Journal of Quantitative Spectroscopy and Radiative Transfer, 138, 36–49, 2014.

Wielicki, B., Barkstrom, B., Harrison, E., Lee III, R., Louis Smith, G., and Cooper, J.: Clouds and the Earth's Radiant Energy System (CERES): An earth observing system experiment, Bulletin of the American Meteorological Society, 77, 853–868, 1996.

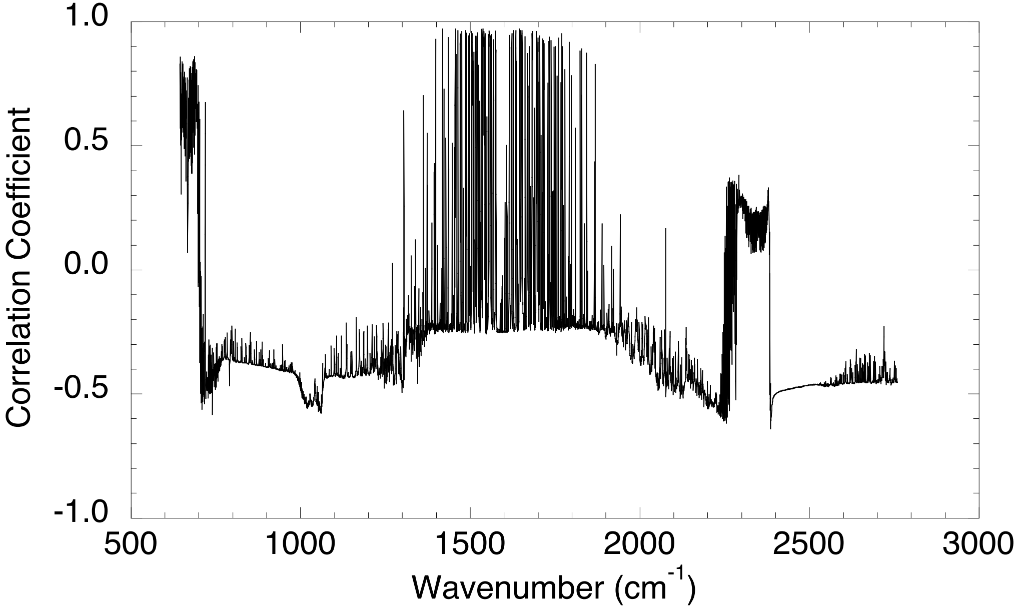

Figure 1. Linear correlation coefficients between the radiance at 25.25 cm^{-1} and the rest of the spectrum. Data is simulated by the LBLRTM from Phillips Soundings.

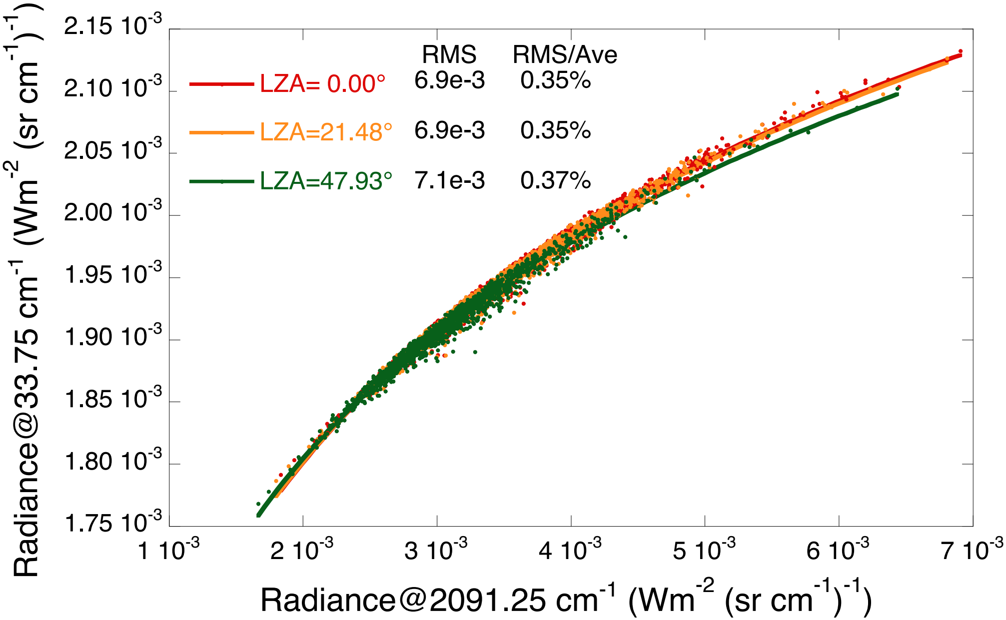

Figure 2. Relationship of radiances at 33.75 cm^{-1} and 2091.25 cm^{-1} simulated by LBLRTM from Phillips Soundings, where the scatter points and fitting curve are based on data for local zenith ~~angle~~ angles (LZA) of 0° (red), 21.48° (orange), and 47.93° (green), respectively. Units are $Wm^{-2}sr^{-1}(cm^{-1})^{-1}$.

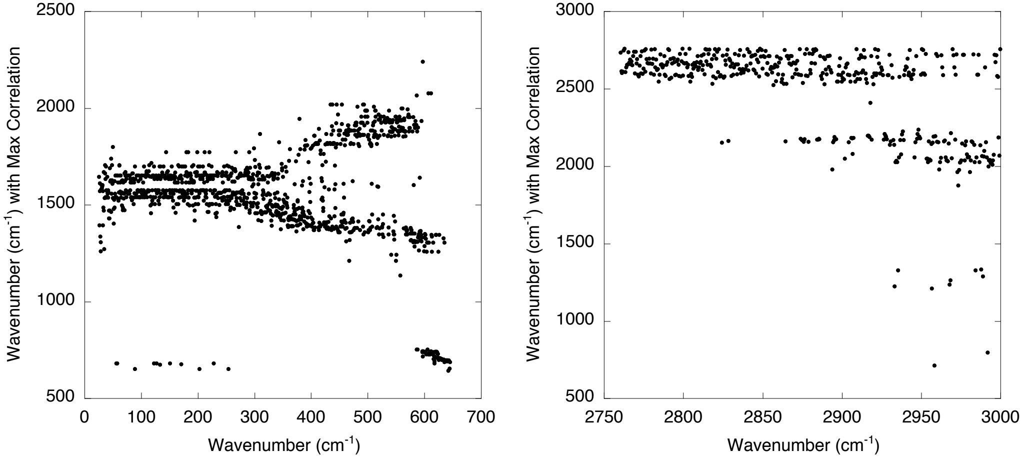

Figure 3. The wavenumbers of IASI observed radiance spectrum (y-axis) that show empirically the maximum correlation coefficients for the FIR (left) and NIR (right) wavenumbers (x-axis), based on a log-log transformation.

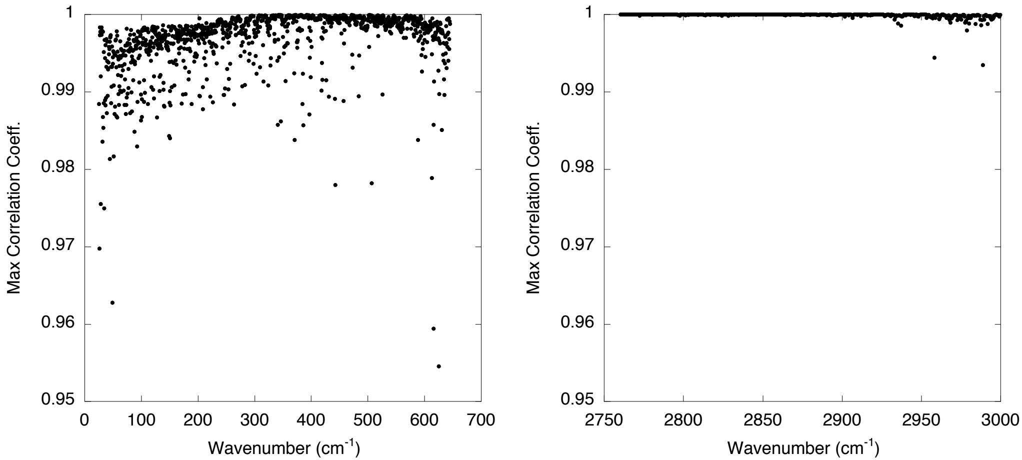

Figure 4. The maximum correlation coefficients between wavenumbers in the FIR (left) and NIR (right) and the corresponding predictor wavenumbers shown in Figure 3.

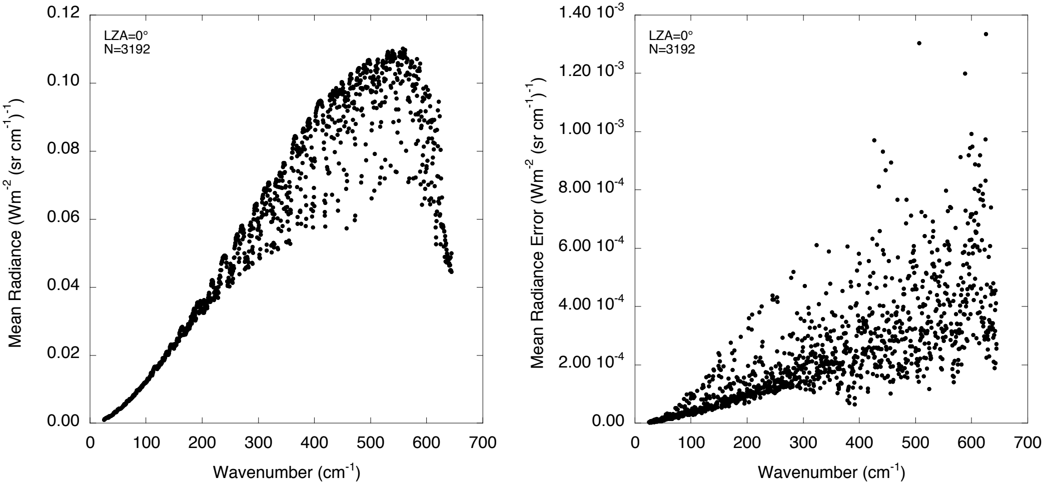

Figure 5. The mean FIR radiance spectrum based on all LBLRTM simulations performed with the 3192 radiosonde profiles (left), and the spectral radiance estimation errors (regression rms errors) associated with them (right). All simulations shown are for a local zenith angle of 0°.

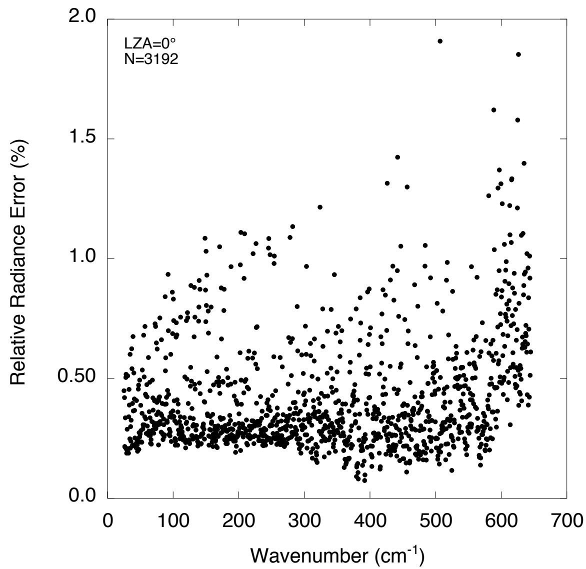

Figure 6. Relative radiance estimation error for the FIR region. Calculated from the root mean square values of the radiance errors divided by the mean radiance spectrum (the right and left plots of Figure 5 respectively).

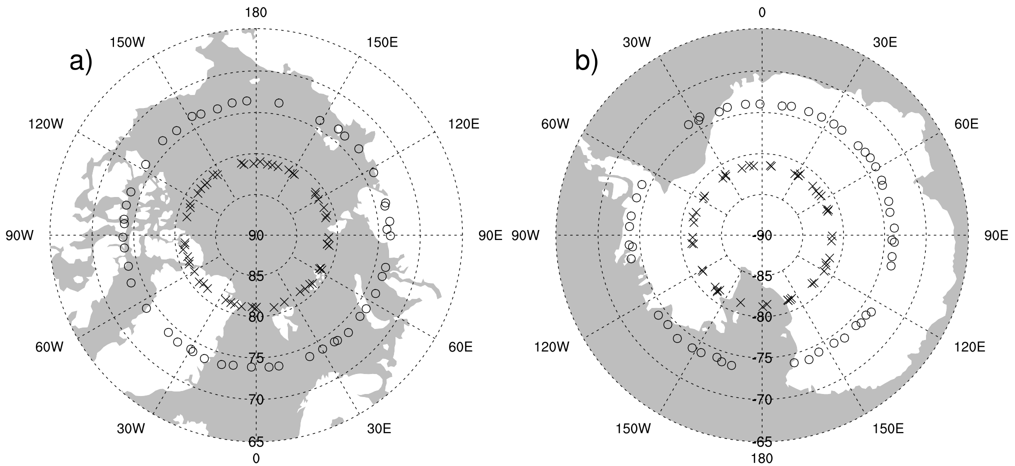

Figure 7. Locations of nearest nadir viewing SNOs, chosen as described in section 2.4 between Metop-A and Terra (inner crosses) and Aqua (outer circles) for a) the Arctic, and b) Antarctic, for 2012.

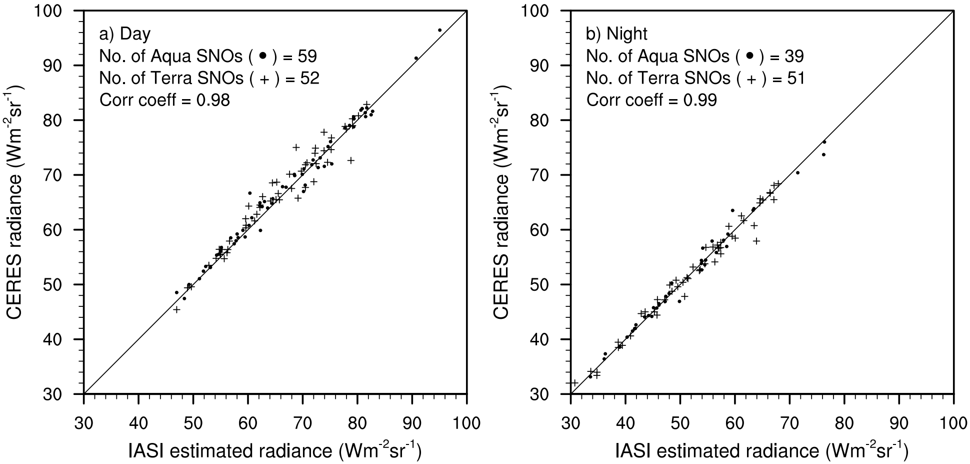

Figure 8. Absolute values of ~~instantaneous LW radiances~~ INLR constructed from IASI on Metop-A against CERES measurements for both the Terra and Aqua satellites at closest SNO events for 2012 for a) day, and b) night.

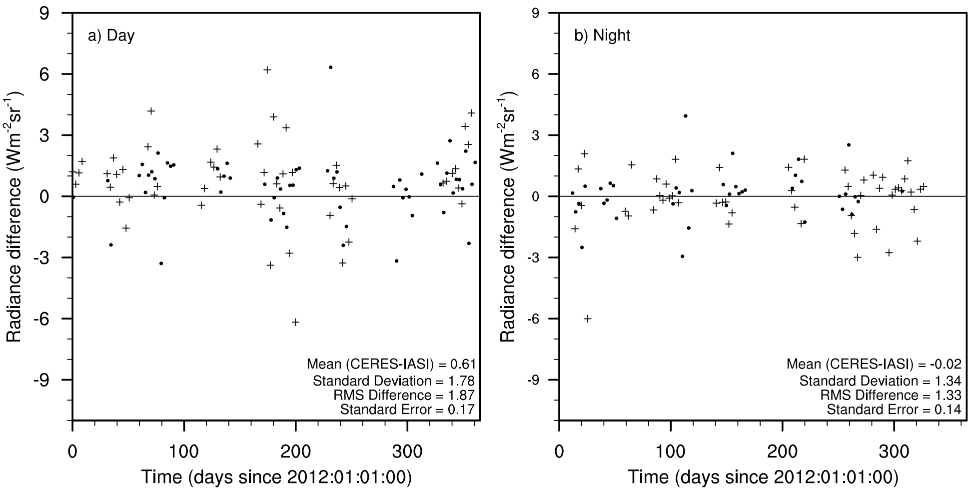

~~Differences between monthly gridded and averaged total LW radiances (CERES - IASI) at all available local times in April 2012 for: a) Aqua all-sky, b) Aqua clear-sky, c) Terra all-sky, and d)Terra clear-sky. Zonal means are shown to~~ Standard error is the ~~right. Units are Wm^{-2}sr^{-1}. Figures in brackets are relative differences between~~ standard deviation divided by the ~~bias and~~ square root of the ~~mean radiation measured by both CERES and IASI~~total number of points.

~~Differences between monthly gridded and averaged total LW radiances (CERES - IASI) at all available local times in April 2012 for: a) Aqua all-sky, b) Aqua clear-sky, c) Terra all-sky, and d)Terra clear-sky. Zonal means are shown to~~ Standard error is the ~~right. Units are Wm^{-2}sr^{-1}. Figures in brackets are relative differences between~~ standard deviation divided by the ~~bias and~~ square root of the ~~mean radiation measured by both CERES and IASI~~total number of points.

Figure 9. Time series of ~~LW radiance~~ INLR bias at SNOs between CERES and IASI for 2012 for a) day and b) night. CERES measurements from Terra are marked with crosses and those from Aqua are shown as dots.

~~Differences between monthly gridded and averaged total LW radiances (CERES - IASI) at all available local times in April 2012 for: a) Aqua all-sky, b) Aqua clear-sky, c) Terra all-sky, and d)Terra clear-sky. Zonal means are shown to~~ Standard error is the ~~right. Units are $Wm^{-2}sr^{-1}$. Figures in brackets are relative differences between~~ standard deviation divided by the ~~bias and~~ square root of the ~~mean radiation measured by both CERES and IASI~~total number of points.

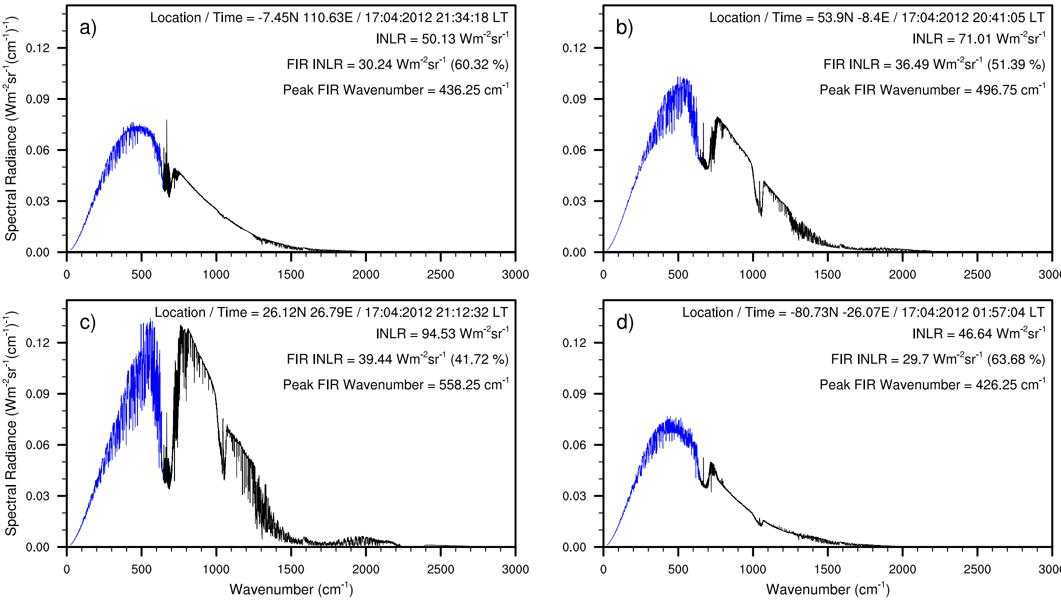

Figure 10. The total outgoing longwave spectral radiance (25.25 - 2999.75 cm^{-1}) constructed from IASI measurements (black) and estimated far infrared radiances (blue) for 4 instantaneous scenes over: a) tropical ~~rainforest~~equatorial land, b) midlatitude land, c) the Sahara desert, and d) Antarctica. All are night-time scenes from the ~~7th~~ 17th April 2012.

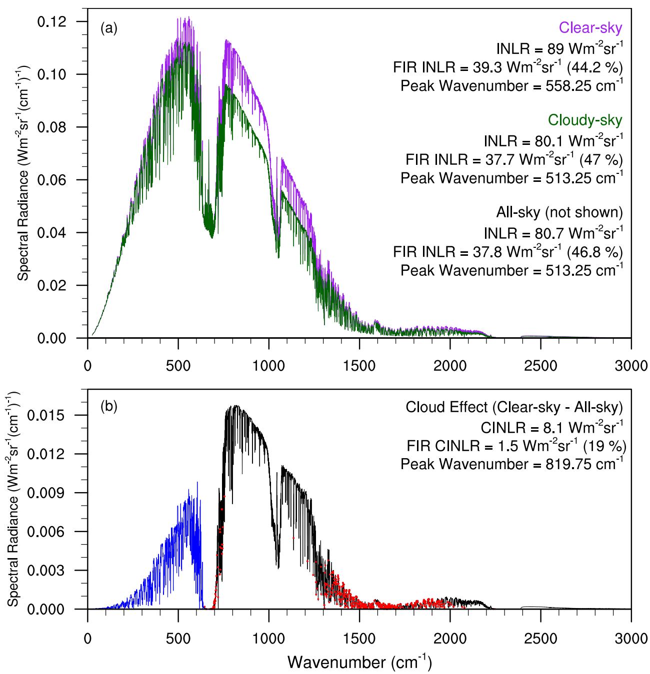

Figure 11. The outgoing longwave spectral radiance constructed from IASI data globally averaged for: a) clear (purple) and cloudy (green) pixels. Numbers in parentheses are the fractional FIR contributions to the total LW broadband ~~OLR~~INLR. The all-sky curve ~~would lie~~ is between the clear and cloudy curves but is not plotted for clarity. b) The difference between the clear-sky and all-sky ~~(CRF)~~ spectrum's constructed from IASI measurements (black) and estimated far infrared radiances (blue) from predictor wavelengths in the mid infrared with the highest correlations (red dots). The number in parentheses is the fractional contribution of the FIR ~~CRF~~ INLR (FIR CINLR) to the total ~~LW broadband CRF~~INLR (CINLR). Data is the area weighted ~~monthly~~ mean of April 2012.

~~outgoing LW radiance maps created from all April 2012 pixels binned to a 2.5 by 2.5 grid and averaged. Zonal means are shown to the right of each map. On the left hand side we have all-sky: a) total OLR, c) FIR as a percentage of OLR, e) window region as a percentage of OLR. On the right we have CRF (clear-sky - all-sky) for: b) OLR, d) the percentage of OLR that is FIR in the CRF, f) the percentage of OLR that is in the window region in the CRF. Note that the colour scales are different for every panel. Missing data is shown in~~

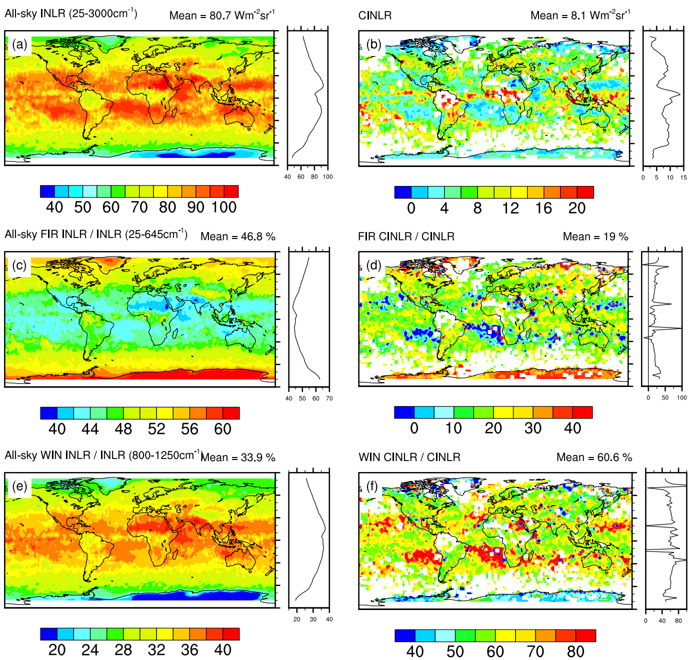

~~white.~~

Figure 12. INLR and CINLR maps created from all April 2012 pixels binned to a 2.5 by 2.5 grid and averaged. Zonal means are shown to the right of each map. On the left hand side is all-sky: a) INLR, c) FIR as a percentage of INLR, e) the window region as a percentage of INLR. On the right is CINLR (clear-sky - all-sky) for: b) INLR, d) the percentage of CINLR that is FIR, f) the percentage of CINLR that is in the window region. Note that the colour scales are different for every panel. Missing data is shown in white.

Table 1. Instantaneous biases between CERES and IASI ~~OLR~~ INLR at SNO events with standard errors. Standard errors are the standard deviations divided by the square root of the total number of points. Units are $Wm^{-2}sr^{-1}$. Figures in brackets are relative differences between the bias and the mean radiation measured by both CERES and IASI.

	All times	Day	Night
Both	0.33 ±0.11 (0.50%)	0.61 ±0.17 (0.95%)	-0.02 ±0.14 (0.01%)
Aqua	0.33 ±0.14 (0.57%)	0.48 ±0.20 (0.78%)	0.11 ±0.19 (0.25%)
Terra	0.32 ±0.18 (0.50%)	0.76 ±0.28 (1.15%)	-0.12 ±0.2 (-0.17%)

~~Global mean biases between IASI OLR and CERES instruments for April 2012. Units are $Wm^{-2}sr^{-1}$. Figures in brackets are relative differences between the bias and the mean radiation measured by both CERES and IASI. Italic figures in brackets are the biases split by land and ocean respectively. All times Day Night All-sky 0.79 (0.94%) 1.44 (1.65%) 0.16 (0.18%) Clear-sky 1.14 (1.03%) 3.03 (3.00%) 0.46 (0.22%) All-sky 1.04 (1.26%) 1.40 (1.65%) 0.70 (0.87%) Clear-sky 1.23 (1.23%) 1.80 (1.81%) 1.16 (1.15%) All-sky 0.26 (0.32%) -0.04 (-0.01%) 0.54 (0.69%) Clear-sky 0.08 (0.17%) 1.28 (1.27%) 0.72 (0.94%)~~